bioRxiv preprint doi: https://doi.org/10.1101/766501; this version posted September 12, 2019. The copyright holder for this preprint (which was not certified by peer review) is the author/funder, who has granted bioRxiv a license to display the preprint in perpetuity. It is made available under aCC-BY-NC-ND 4.0 International license.

Fgf-driven Tbx protein activities directly induce *myf5* and *myod* to initiate zebrafish myogenesis

Daniel P.S. Osborn*‡ORCID, Kuoyu Li*§, Stephen J. CuttyORCID, Andrew C. Nelson¶ORCID, Fiona C. WardleORCID, Yaniv HinitsORCID and Simon M. Hughes[1]ORCID

Randall Centre for Cell and Molecular Biophysics, New Hunt's House, Guy's Campus, King's College London, SE1 1UL, UK.

Current addresses:

‡ Cell Biology and Genetics Research Centre, St George's University of London, London SW17 0RE

§ China Zebrafish Resource Centre, Institute of Hydrobiology, Chinese Academy of Sciences, Wuhan, China

¶ School of Life Sciences, Gibbet Hill Campus, University of Warwick, Coventry, CV4 7AL, UK.

Running title: Function of zebrafish MRFs

Keywords: muscle, zebrafish, myosin, myod, myf5, myogenin, hedgehog, fgf, spt, tbx16, ntl, Tbxta

* These authors contributed equally.

[1]Corresponding author: Simon M. Hughes, Randall Division, 3rd floor north, New Hunt's House, Guy's Campus, King's College London, London SE1 1UL, UK. Tel.: +44 20 7848 6445 e-mail: s.hughes@kcl.ac.uk

bioRxiv preprint doi: https://doi.org/10.1101/766501; this version posted September 12, 2019. The copyright holder for this preprint (which was not certified by peer review) is the author/funder, who has granted bioRxiv a license to display the preprint in perpetuity. It is made available under aCC-BY-NC-ND 4.0 International license.

Abstract

Skeletal muscle derives from dorsal mesoderm that is formed during vertebrate gastrulation. Fibroblast growth factor (Fgf) signalling is known to cooperate with transcription factors of the Tbx family to promote dorsal mesoderm formation, but the role of these proteins in skeletal myogenesis has been unclear. Using the zebrafish, we show that dorsally-derived Fgf signals act through Tbx16 and Tbxta to induce two populations of slow and fast trunk muscle precursors at distinct dorsoventral positions. Tbx16 binds to and directly activates the *myf5* and *myod* genes that are required for commitment to skeletal myogenesis. Tbx16 activity depends on Fgf signalling from the organiser. In contrast, Tbxta is not required for *myf5* expression. However, Tbxta binds to a specific site upstream of *myod* not bound by Tbx16, driving *myod* expression in the adaxial slow precursors dependent upon Fgf signals, thereby initiating muscle differentiation in the trunk. After gastrulation, when similar muscle cell populations in the post-anal tail are generated from the tailbud, declining Fgf signalling is less effective at initiating adaxial myogenesis, which is instead initiated by Hedgehog signalling from the notochord. Our findings provide insight into the ancestral vertebrate trunk myogenic pattern and how it was co-opted during tail evolution to generate similar muscle by new mechanisms.

Introduction

Sarcomeric muscle arose early in animal evolution, creating a defining feature of the metazoa: efficient multicellular movement. Prior to protostome-deuterostome divergence, the bilaterian animal likely acquired sensorimotor specializations, including divisions between cardiac, skeletal/somatic and visceral muscles, which are today regulated by similar gene families in Drosophila and vertebrates e.g. *mef2* genes (Taylor and Hughes, 2017). Skeletal myogenesis is initiated during gastrulation, shortly after mesendoderm formation, but conserved bilaterian pathways leading specifically to skeletal muscle (as opposed to cardiac or visceral) have been harder to discern. One likely reason for this is that new regulatory steps have evolved in each lineage since their divergence.

A key step in vertebrate evolution was the chordate transition through which animals acquired the notochord, post-anal tail, gill slits and a more complex dorsal nerve cord,

bioRxiv preprint doi: https://doi.org/10.1101/766501; this version posted September 12, 2019. The copyright holder for this preprint (which was not certified by peer review) is the author/funder, who has granted bioRxiv a license to display the preprint in perpetuity. It is made available under aCC-BY-NC-ND 4.0 International license.

facilitating swimming (Brunet et al., 2015; Gee, 2018; Gerhart, 2001; Satoh et al., 2012). Throughout vertebrates, the notochord patterns the neural tube and paraxial mesodermal tissue by secreting Hedgehog (Hh) signals that promote motoneuron and early muscle formation (Beattie et al., 1997; Blagden et al., 1997; Du et al., 1997; Münsterberg et al., 1995; Roelink et al., 1994). Nevertheless, in the absence of either notochord or Hedgehog signalling, muscle is formed in vertebrate somites (Blagden et al., 1997; Dietrich et al., 1999; Du et al., 1997; Grimaldi et al., 2004; Zhang et al., 2001). How might deuterostome muscle have formed prior to evolution of the notochord?

A change in function of the *Tbxt* gene, a T-box (Tbx) family paralogue, occurred during chordate evolution such that *Tbxt* now directly controls formation of posterior mesoderm, notochord and post-anal tail in vertebrates (Chiba et al., 2009; Showell et al., 2004). Hitherto, *Tbxt* may have distinguished ectoderm from endoderm and regulated formation of the most posterior mesendoderm (Arenas-Mena, 2013; Kispert et al., 1994; Woollard and Hodgkin, 2000; Yasuoka et al., 2016). In vertebrates, *Tbxt* genes also promote slow myogenesis (Coutelle et al., 2001; Halpern et al., 1993; Martin and Kimelman, 2008; Weinberg et al., 1996). Other Tbx genes, such as *Tbx1*, *Tbx4*, *Tbx5*, *Tbx16* and *Tbx6*, also influence sarcomeric muscle development (Chapman and Papaioannou, 1998; Griffin et al., 1998; Hasson et al., 2010; Kimmel et al., 1989; Manning and Kimelman, 2015; Weinberg et al., 1996; Windner et al., 2015). For example, the Tbx6 family is implicated in early stages of paraxial mesoderm commitment, somite patterning and the generation and positioning of muscle precursor cells (Bouldin et al., 2015; Chapman and Papaioannou, 1998; Kimmel et al., 1989; Manning and Kimelman, 2015; Nikaido et al., 2002; White et al., 2003; Windner et al., 2012). It is unclear, however, whether the Tbx genes promote myogenesis directly, and/or are required for earlier events in mesoderm development that are necessary for subsequent myogenesis.

In vertebrates, a key essential step in skeletal myogenesis is activation of myogenic regulatory factors (MRFs) encoded by the *myf5* and *myod* genes (Hinits et al., 2009; Hinits et al., 2011; Rudnicki et al., 1993). Distinct myogenic cell populations initiate *myf5* and *myod* expression in different ways, the genes being induced by distinct signals through distinct *cis*-regulatory elements in different skeletal muscle precursor cells (Buckingham and Rigby, 2014). As the anteroposterior axis forms and extends, *de novo* induction of *myf5* and *myod* mRNAs in slow and fast muscle precursors occurs in tissue destined to generate each successive somite. Once expressed, these MRF proteins have two

bioRxiv preprint doi: https://doi.org/10.1101/766501; this version posted September 12, 2019. The copyright holder for this preprint (which was not certified by peer review) is the author/funder, who has granted bioRxiv a license to display the preprint in perpetuity. It is made available under aCC-BY-NC-ND 4.0 International license.

functions: to remodel chromatin and directly enhance transcription of muscle genes (reviewed in (Buckingham and Rigby, 2014). In zebrafish, myogenesis begins at about 75% epiboly stage when adaxial cells that flank the shield/organizer/nascent notochord (hereafter called pre-adaxial cells; diagrammed in Fig. 1A), begin MRF expression (Hinits et al., 2009; Melby et al., 1996). Pre-adaxial cells express both *myf5* and *myod*, converge to form two rows of adaxial cells flanking the notochord, become incorporated into somites and differentiate into slow muscle fibres (Coutelle et al., 2001; Devoto et al., 1996; Weinberg et al., 1996). Loss of either Myf5 or Myod alone is not sufficient to prevent slow myogenesis, but loss of both completely inhibits adaxial slow muscle formation (Hinits et al., 2009; Hinits et al., 2011). Dorsal tissue immediately lateral to the pre-adaxial cells, the paraxial mesoderm (Fig. 1A), expresses *myf5* but little *myod* and subsequently generates fast muscle once somites have formed, upregulating *myod* in the process. A key to understanding myogenesis in both paraxial and adaxial cells is thus the mechanism(s) by which *myf5* and *myod* expression is regulated.

Intrinsic factors such as Tbx proteins likely interact with extrinsic positional cues within the embryo to pattern myogenesis. Fgf and Tbx function have long been known to interact to drive early mesendoderm patterning, but how directly they control early embryonic myogenesis remains unclear (Kimelman and Kirschner, 1987; Showell et al., 2004; Slack et al., 1987). Various Fgf family members are expressed close to myogenic zones during vertebrate gastrulation (Isaacs et al., 2007; Itoh and Konishi, 2007; Wilkinson et al., 1988). In zebrafish, Fgf signalling is required for mesendoderm formation, tailbud outgrowth and normal fast myogenesis (Draper et al., 2003; Griffin et al., 1995; Groves et al., 2005; Reifers et al., 1998; Yin et al., 2018). Fgf signalling is also thought to be involved in early expression of *myf5* and *myod* in pre-adaxial cells, but the mechanism of initial induction of *myf5* and *myod* is unknown (Ochi et al., 2008). Expression of *fgf3*, *fgf4*, *fgf6a*, *fgf8a* and *fgf8b* has been detected in the chordoneural hinge (CNH, Fig. 1A) adjacent to pre-adaxial cells (Draper et al., 2003; Groves et al., 2005; Thisse and Thisse, 2005). Subsequently, Hedgehog (Hh) signalling from the ventral midline maintains MRF expression and progression of the pre-adaxial cells into terminal slow muscle differentiation (Coutelle et al., 2001; Hirsinger et al., 2004; Lewis et al., 1999). Here, we show how both Fgf and Hh extracellular signals cooperate with Tbx genes to control fast and slow myogenesis. In the trunk, Fgf signalling is required for the initiation of myogenesis and acts in cooperation with Tbx16/Tbxta function directly on *myf5* and *myod*. In the tail, by contrast, direct MRF gene

bioRxiv preprint doi: https://doi.org/10.1101/766501; this version posted September 12, 2019. The copyright holder for this preprint (which was not certified by peer review) is the author/funder, who has granted bioRxiv a license to display the preprint in perpetuity. It is made available under aCC-BY-NC-ND 4.0 International license.

induction by Fgf is not required and the evolutionary novelty of midline-derived Hh-signalling accounts for adaxial myogenesis.

Results

Fgf signalling is essential for induction of adaxial myf5 and myod expression

Adaxial myogenesis is driven by successive Fgf and Hh signals. When Hh signalling was prevented with the Smo antagonist cyclopamine (cyA), *myf5* and *myod* mRNAs in pre-adaxial cells were unaffected at 90% epiboly (Fig. 1A). In contrast, when Fgf signalling was inhibited with SU5402 both *myf5* and *myod* mRNAs were lost (Fig. 1A)(Ochi et al., 2008). To show that lack of MRFs was not due to failure of gastrulation caused by SU5402-treatment, we analysed expression of *aplnrb* mRNA, an anterior mesodermal marker (Zeng et al., 2007). At 80% epiboly, *aplnrb* mRNA has a complex and informative expression pattern, marking the anterior invaginating mesoderm cells around the germ ring and the pre-adaxial cells, but appears down-regulated in more lateral regions expressing *myf5* but not *myod* (Figs 1A; S1, see Table S1 for quantification of this and subsequent experiments). In SU5402-treated embryos, *aplnrb* mRNA reveals the normal invagination of mesoderm and *aplnrb*-expressing cells flanking the organiser. Both the downregulation of *aplnrb* mRNA in paraxial trunk mesoderm that normally expresses *myf5* alone, and pre-adaxial *aplnrb* up-regulation were absent in SU5402-treated embryos (Fig. 1A). Thus, early Fgf signalling is required for the initiation of skeletal myogenesis in future trunk regions.

As trunk myogenesis proceeds, Hh signalling becomes essential for adaxial slow myogenesis. At 6ss, in *smo* mutants, cyA-treated embryos and even cyA-treated *smo* mutants, all of which lack Hh signalling, *myod* mRNA is lost from adaxial slow muscle but persists in paraxial fast muscle precursors (Fig. 1B). Nevertheless, *myod* mRNA transiently accumulates in pre-adaxial cells of presomitic mesoderm (PSM) destined to make trunk somites, but is then lost in anterior PSM (Fig. 1B)(Barresi et al., 2000; Lewis et al., 1999; Osborn et al., 2011; van Eeden et al., 1996; van Eeden et al., 1998). Thus, as suggested previously (Coutelle et al., 2001; Ochi et al., 2008), in the wild type situation trunk pre-adaxial *myod* expression is maintained and enhanced by Hh. In contrast, during tail myogenesis at 15ss and thereafter, no pre-adaxial *myod* expression was detected in *smo* mutants or cyA-treated embryos (Fig. 1B and data not shown). These data suggest

bioRxiv preprint doi: https://doi.org/10.1101/766501; this version posted September 12, 2019. The copyright holder for this preprint (which was not certified by peer review) is the author/funder, who has granted bioRxiv a license to display the preprint in perpetuity. It is made available under aCC-BY-NC-ND 4.0 International license.

that whereas Hh is necessary for induction of adaxial myogenesis in the tail, Fgf-like signals initiate *myod* expression in trunk pre-adaxial cells.

Additional evidence emphasizes the greater importance of Hh in tail myogenesis. In *shha* mutants, slow muscle is lost from tail but remains present in trunk somites (Fig. 2A). Moreover, injection of *myod* or *myog* mRNA into embryos lacking Hh signalling can rescue slow myogenesis in trunk but not in tail (Fig. S2). Similarly, absence of notochord-derived signals in *noto* (*flh*) mutants, in which the nascent notochord loses notochord character and converts to muscle (Coutelle et al., 2001; Halpern et al., 1995), ablates tail but not trunk slow muscle (Fig. 2B). Treatment of *noto* mutants with cyA shows that *myod* expression is initiated in trunk pre-adaxial cells adjacent to the transient pre-notochordal tissue, but fails to be maintained owing to the blockade of floorplate-derived Hh signals (Fig. 2C). Taken together, these data show that Hh can initiate and then maintain MRF gene expression, but that other signals initiate slow myogenesis in the trunk.

We next tested whether Hh-independent *myod* expression and *myf5* up-regulation in trunk pre-adaxial cells requires Fgf signalling. Treatment with cyA left residual pre-adaxial *myod* and *myf5* mRNA flanking the base of the notochord at trunk levels, but ablated adaxial expression in slow muscle precursor cells (Fig.2D). The residual expression was ablated when, in addition to cyA, SU5402 was used to block *fgf* signalling from 30% epiboly (Fig. 2D). Application of SU5402 alone diminished *myf5* and *myod* mRNA accumulation up to tailbud stage, but caused little if any reduction of adaxial *myf5* and *myod* mRNAs in the tailbud region at the 6 somite stage (6ss), after midline *shha* function had commenced (Fig. 1B,C)(Krauss et al., 1993). Nevertheless, SU5402 greatly diminished *myod* expression in somitic fast muscle precursors and reduced the extent of *myf5* expression in paraxial PSM (Fig. 1B,C)(Groves et al., 2005; Reifers et al., 1998).

Fgf3, fgf4, fgf6a and fgf8a collaborate to promote MRF expression

To identify candidate Fgf regulators of pre-adaxial myogenesis, the expression patterns of *fgf3*, *fgf4*, *fgf6a* and *fgf8a* were investigated on wild type embryos (Fig. S3A). As reported previously, *fgf4*, *fgf6a* and *fgf8a* mRNAs were all detected in the posterior dorsal midline at 80% epiboly, followed by *fgf3* in the chordoneural hinge (CNH) and posterior notochord (Fig. S3A)(Kudoh et al., 2001; Thisse and Thisse, 2005; Yamauchi et al., 2009). The temporal and spatial expression of *fgf3*, *fgf4*, *fgf6a* and *fgf8a* during gastrulation and early

bioRxiv preprint doi: https://doi.org/10.1101/766501; this version posted September 12, 2019. The copyright holder for this preprint (which was not certified by peer review) is the author/funder, who has granted bioRxiv a license to display the preprint in perpetuity. It is made available under aCC-BY-NC-ND 4.0 International license.

somitogenesis make them excellent candidates for Fgf regulators of *myf5* and *myod*.

To evaluate the role of Fgfs in *myf5* and *myod* expression, each Fgf was knocked down with previously validated antisense morpholino oligonucleotides (MOs) in wild type embryos (Fig. S3B). At 80% epiboly, there was little or no decrease of *myf5* or *myod* mRNA in individual *fgf* morphants or *fgf8a* mutant embryos (Fig. S3B). Combinatorial knockdown of several fgfs led to progressively more severe loss of *myod* mRNA and reduction of the raised pre-adaxial and paraxial levels of *myf5* mRNA (Fig. 3A). Thus, specific Fgfs collaborate to drive the initial expression of *myod* and *myf5* in pre-adaxial and paraxial cells.

By tailbud stage, however, *fgf4+fgf8a* MO treatment alone had little effect on *myod* mRNA accumulation, presumably due to the presence of Hh in the midline (Fig. 3B). Congruently, cyA-treatment reduced anterior adaxial *myod* mRNA, but pre-adaxial expression persisted after blockade of Hh signalling (Fig. 3B). Pre-adaxial *myod* mRNA was ablated by cyA-treatment of embryos injected with *fgf4+fgf8a* MO (Fig. 3B). Control injection of *fgf4+fgf8a* MOs into vehicle-treated embryos did not reduce *myod* mRNA accumulation, confirming that Hh can initiate trunk adaxial *myod* expression (Fig. 3B). Thus, expression of Fgf4 and Fgf8a in the shield, CNH and posterior notochord, provides a spatiotemporal cue for pre-adaxial myogenic initiation in the tailbud.

To test the ability of Fgfs to promote myogenesis further, we generated ectopic Fgf signals by injection of *fgf4* or *fgf6a* mRNA into wild type embryos, and analysed *myf5* and *myod* mRNA at 80% epiboly (Fig. 3C). Both *myod* and *myf5* mRNAs were upregulated in more ventral regions at levels comparable to those in adaxial cells of control embryos, despite the absence of Hh signalling in these regions. Over-expression of *fgf4* mRNA upregulated *myf5* mRNA in an initially uniform band around the embryo that extended towards the animal pole for a distance similar to that of *myod* mRNA in adaxial cells of controls (Fig. 3C). *Myod* was less easily induced, but in similar regions of the mesoderm. The posterior notochord and shield still lacked MRFs and appeared wider. However, this dorsalmost tissue was not enlarged; the number of notochord cells scored by DAPI stain appeared normal (data not shown). The embryos became ovoid, with a constriction around the germ ring that appeared to stretch and broaden the notochord. There was a positive correlation between the extent of *myf5* and *myod* mRNA up-regulation and the extent of deformation towards egg-shape. *Aplnrb* mRNA persisted in animal regions of the mesoderm, but was downregulated where *myf5* mRNA was induced nearer to the margin, revealing that

bioRxiv preprint doi: https://doi.org/10.1101/766501; this version posted September 12, 2019. The copyright holder for this preprint (which was not certified by peer review) is the author/funder, who has granted bioRxiv a license to display the preprint in perpetuity. It is made available under aCC-BY-NC-ND 4.0 International license.

anterior/cranial mesoderm is present but resistant to Fgf-driven MRF induction and *aplnrb* suppression (Fig. 3D). Thus, Fgf4 dorsalized the embryo, converting the entire posterior paraxial and ventral mesoderm to a myogenic profile with some regions expressing only *myf5* and others expressing also *myod*, particularly around the germ ring. Fgf6a overexpression also induced ectopic MRFs in cells around the germ ring, which then appeared to cluster (Fig. 3C). Taken together, these data show that posterior/dorsal Fgf signals initiate MRF expression in both pre-adaxial slow and paraxial fast muscle precursors in pre-somitic mesoderm.

MRFs are initially induced by fgfs, tbxta and tbx16

Zebrafish Tbx genes, including *tbxta* and *tbx16* (formerly called *no tail* (*ntla*) and *spadetail* (*spt*), respectively), are potentially important mediators of Fgf signalling in gastrulating embryos (Amaya et al., 1993; Griffin et al., 1995; Smith et al., 1991; Sun et al., 1999). *Tbx16* is suppressed by a dominant negative Fgf receptor (FgfR) (Griffin et al., 1998). However, whether *tbxta* and *tbx16* activities are altered by SU5402 treatment, which also blocks FgfR function, is unclear (Rentzsch et al., 2004; Rhinn et al., 2005). Wild type embryos at 30% epiboly were therefore exposed to SU5402 and subsequently fixed at 80% epiboly or 6ss to investigate expression of *tbxta and tbx16* (Fig. 4A). Compared to controls, embryos treated with 10 µM SU5402 showed diminished *tbxta* expression in notochord and less *tbxta* and *tbx16* in the germ ring, particularly in dorsal paraxial regions. At 6ss, expression of *tbxta* and *tbx16* was mildly reduced in tailbud by 10 µM SU5402 (Fig. 4A). When the concentration of SU5402 was increased to 30 µM, expression of *tbxta* and *tbx16* was abolished throughout the trunk (Fig. 4A). Thus, Fgf-like signalling is required for normal Tbx gene expression in the mesoderm.

Tbxta is required for normal *myf5* and *myod* expression in posterior regions during tailbud outgrowth, partly due to loss of Hh signalling from the missing notochord (Coutelle et al., 2001; Weinberg et al., 1996). To test whether Tbx genes are required for MRF expression at earlier stages, each Tbx gene was knocked down and MRF and Fgf expression analysed at 80% epiboly. Tbxta knockdown reduced expression of dorsal midline Fgfs, ablated *myod* mRNA and reduced *myf5* mRNA accumulation in pre-adaxial cells to the level in paraxial regions (Fig. 4B). However, Tbxta knockdown had little effect on either *fgf8a* or *myf5* mRNAs in more lateral paraxial mesoderm or the germ ring (Fig. 4B). This

bioRxiv preprint doi: https://doi.org/10.1101/766501; this version posted September 12, 2019. The copyright holder for this preprint (which was not certified by peer review) is the author/funder, who has granted bioRxiv a license to display the preprint in perpetuity. It is made available under aCC-BY-NC-ND 4.0 International license.

correlation raised the possibility (addressed below) that Tbxta may drive MRF expression through induction of Fgf expression. Tbx16 knockdown, on the other hand, ablated pre-adaxial *myod* mRNA and reduced both pre-adaxial and paraxial *myf5* mRNA without reduction of Fgf expression (Fig. 4B). Indeed, both germ ring *fgf8a* mRNA at 80% epiboly and dorsal midline *fgf3*, *fgf4* and *fgf8a* mRNAs in the tailbud at 6ss appeared increased (Fig. 4B), as previously described (Warga et al., 2013). As Tbx16 expression persists in *tbxta* mutants (Amack et al., 2007; Griffin et al., 1998), these data raise the possibility that Tbx16 is required to mediate the action of Fgf signals on myogenesis.

Tbx16 null mutants show a failure of convergent migration of mesodermal cells into the paraxial region (Ho and Kane, 1990; Molven et al., 1990) which, by reducing mesodermal cells flanking the CNH, may contribute to the reduction in MRF mRNAs observed at 80% epiboly. Nevertheless, *tbx16* mutants generate enough paraxial mesoderm that reduced numbers of both paraxial fast muscle and adaxially-derived slow muscle fibres arise after Hh signalling commences (Honjo and Eisen, 2005; Weinberg et al., 1996). To investigate whether Tbx16 is required for initial induction of *myf5* and/or *myod* expression in pre-adaxial cells, we titrated MO to reduce *tbx16* function to a level that did not prevent accumulation of significant numbers of trunk mesodermal cells and examined *myf5* and *myod* expression at 6ss (Fig. 4C). In *tbx16* morphants, *myod* mRNA was readily detected in adaxial cells adjacent to notochordal Hh expression (Fig. 4C, cyan arrowheads). Treatment of these *tbx16* morphants with cyA to block Hh signalling, however, completely ablated adaxial *myod* expression, leaving only weak *myod* in paraxial somitic fast muscle precursors (Fig. 4C, cyan and purple arrowheads). In contrast, treatment of control embryos with cyA left pre-adaxial *myod* mRNA intact (Fig. 4C, black arrowheads). These findings show that Fgf-driven pre-adaxial *myod* expression flanking the CNH requires Tbx16 function.

Adaxial *myf5* expression also requires Tbx16. Tbx16 knockdown reduces *myf5* mRNA accumulation in the posterior tailbud, and also diminishes the upregulation of *myf5* mRNA in pre-adaxial and adaxial cells (Fig. 4C, orange arrowheads). Addition of cyA to *tbx16* morphants has little further effect on *myf5* expression (Fig. 4C, white arrowheads). In contrast, cyA treatment alone reduces adaxial *myf5* mRNA in anterior PSM, but does not affect the *myf5* up-regulation in pre-adaxial cells or tailbud *myf5* expression (Fig. 4C, white arrowheads). Additional knockdown of Tbx16 in cyA-treated embryos prevents pre-adaxial *myf5* up-regulation (Fig. 4C, white arrowheads). Thus, Tbx16 is required for Fgf to up-

bioRxiv preprint doi: https://doi.org/10.1101/766501; this version posted September 12, 2019. The copyright holder for this preprint (which was not certified by peer review) is the author/funder, who has granted bioRxiv a license to display the preprint in perpetuity. It is made available under aCC-BY-NC-ND 4.0 International license.

regulate both *myf5* and *myod* in pre-adaxial cells.

Both pre-adaxial and anterior PSM adaxial *myod* expression were also absent in *tbxta* morphants, but recovered in somites, again due to midline-derived Hh signalling (Fig. 4C and (Coutelle et al., 2001)). In marked contrast, Tbxta knockdown up-regulated *myf5* mRNA in tailbud (Fig. 4C, asterisk), presumably reflecting loss of tailbud stem cells that lack *myf5* mRNA. Taken together, the data strongly suggest that *tbx16* is required for midline-derived Fgf signals to induce *myod* and up-regulate *myf5* in pre-adaxial cells in tailbud. In contrast, the loss of MRF expression in *tbxta* mutants could be simply explained by loss of midline-derived Fgf signals, and/or might require some other Tbxta-dependent process.

Myf5 and myod induction by Fgf signalling require Tbx16

To test rigorously the idea that Tbx16 is required for Fgf to induce MRFs, *fgf4* mRNA was injected into embryos from a *tbx16* heterozygote incross. Whereas Fgf4 up-regulated *myf5* and *myod* mRNAs all around the germ ring in siblings, in sequence-genotyped *tbx16* mutant embryos no up-regulation was detected (Fig. 5A). It is clear that mesoderm was present in *tbx16* mutants because the mRNAs encoding Aplnrb, Tbxta, Tbx16 and Tbx16-like (formerly Tbx6-like) are present in *tbx16* mutants (Fig. S4; (Griffin et al., 1998; Morrow et al., 2017)). The effect of Fgf4 does not act by radically altering *tbxta* or *tbx16* gene expression (Fig. 5B). Thus, Tbx16 is required for Fgf-driven expression of MRFs in pre-somitic mesoderm.

Tbx16 requires Fgf-like signalling to rescue myf5 and myod expression

The results so far show that *tbx16* function is necessary for Fgf to induce *myf5* and *myod* (Fig. 5A). To determine if increased Tbx16 activity is sufficient to induce MRFs, Tbx16 was overexpressed. Injection of *tbx16* mRNA caused ectopic expression of both *myf5* and *myod* in the germ marginal zone (Fig. 5C). Notably, Tbx16 over-expression induced *myf5* mRNA in a much broader region than *myod* mRNA.

We next wanted to determine whether Tbx16 could induce expression of *myf5* or *myod* in the absence of Fgf signalling. Exposure to high dose SU5402, which down-regulates endogenous *tbx16* and *tbxta* mRNA (Fig. 4A), prevented MRF induction by injection of

bioRxiv preprint doi: https://doi.org/10.1101/766501; this version posted September 12, 2019. The copyright holder for this preprint (which was not certified by peer review) is the author/funder, who has granted bioRxiv a license to display the preprint in perpetuity. It is made available under aCC-BY-NC-ND 4.0 International license.

tbx16 mRNA (Fig. 5D). Nevertheless, when *tbx16* mRNA was injected into low dose (10 μM) SU5402-treated embryos, which normally have reduced MRF expression, the level of *myf5* and *myod* mRNAs was rescued (Fig. 5C). However, *tbx16* mRNA was less effective at ectopic MRF induction in the presence of SU5402 (Fig. 5C). These results demonstrate that Fgf signalling cooperates with Tbx16 activity in inducing expression of *myf5* and *myod* in pre-adaxial cells at gastrulation stages. Moreover, Tbx16 requires Fgf-like signals to induce MRF gene expression.

Myf5 and Myod are direct transcriptional targets of Tbx16

In order to determine further the regulatory relationship between Tbx16 and *myf5* and *myod* we interrogated ChIP-seq experiments for endogenous Tbx16 on 75-85% epiboly stage embryos (see Materials and Methods)(Nelson et al., 2017). Our analyses revealed a highly significant peak at -80 kb upstream (*myf5* Distal Element, 5DE) and two binding peaks proximal to *myf5* (Proximal Elements, 5PE1,5PE3) (Fig. 6A,B and Supplementary Table S3). To determine which of these binding events are likely to be functionally important we further cross-referenced the data with published histone modification ChIP-seq data (Bogdanovic et al., 2012). The 5DE and 5PE1 peaks overlapped significant H3K27ac and H3K4me1 peaks (Table S3), suggesting these are likely to be functionally active enhancers. Tbx16 ChIP-qPCR confirmed the validity of the 5DE and 5PE1 ChIP-seq peaks (Fig. 6C). These putative enhancers are likely to regulate *myf5*, the promoter of which has a H3K4me3 mark, rather than the adjacent *myf6* gene, which is not expressed at 80% epiboly and does not have a H3K4me3 mark. Comparison of the sequences under each peak to genomic regions adjacent to the *myf5* gene in other fish species revealed significant conservation (Figs 6A,B). Of particular note was the conservation of 5DE in medaka and stickleback, while 5PE1 showed notable conservation in medaka and fugu (Figs 6A,B). Thus, ChIP-seq peaks corresponding to histone marks indicative of enhancer activity suggest evolutionarily conserved mechanisms of *myf5* regulation in fish.

We next tested whether Tbx16 is able to positively regulate *myf5* directly. To do this we used a hormone-inducible system to activate Tbx16 in the presence of cycloheximide, followed by *in situ* hybridization (Kolm and Sive, 1995; Martin and Kimelman, 2008). Briefly, mRNA corresponding to Tbx16 fused to the hormone binding domain of glucocorticoid receptor (GR) was overexpressed in wild-type embryos. The resulting

bioRxiv preprint doi: https://doi.org/10.1101/766501; this version posted September 12, 2019. The copyright holder for this preprint (which was not certified by peer review) is the author/funder, who has granted bioRxiv a license to display the preprint in perpetuity. It is made available under aCC-BY-NC-ND 4.0 International license.

protein is held in the cytoplasm until dexamethasone (DEX) stimulates GR nuclear translocation. In the presence of the translation inhibitor cycloheximide (CHD), increased nuclear Tbx16 is expected mosaically to induce only direct targets of Tbx16 (Fig. 6D). Ectopic expression of *myf5* around the germ ring was observed upon Tbx16 activation (Fig. 6E). Moreover, using the same approach, induction of *myod* mRNA indicated that *myod* is also a direct target of Tbx16 (Fig. 6E). *Myod* mRNA up-regulation was, however, restricted to a narrow ectopic domain flanking the base of the notochord, indicating that *myod* expression is under additional Tbx16-independent constraints compared to *myf5* (Fig. 6E). Interestingly, across the set of CHD+DEX-treated embryos, ectopic *myf5* mRNA was induced to a higher level in a similar region to ectopic *myod* mRNA than elsewhere, suggesting that Tbx16 was able to induce two aspects of pre-adaxial character directly in this region of the embryo. To confirm this result, we tested whether Myf5 is required for Tbx16 to induce *myod* expression. When *tbx16* mRNA was injected into *myf5* mutant or heterozygote embryos, ectopic *myod* mRNA was observed flanking the base of the notochord in about 50% of embryos, but appeared more readily induced in wild type siblings (Fig. 6F). Thus, Tbx16 is necessary for MRF expression and can induce both *myf5* and *myod* independently, so long as Fgf signalling is active. In summary, Tbx16 directly induces MRF expression in gastrulating mesoderm and is particularly potent in the pre-adaxial region that normally retains high Tbx16 expression.

Tbxta is essential for pre-adaxial but not paraxial myogenesis

Whereas the entire paraxial PSM expresses *myf5*, pre-adaxial cells upregulate *myf5* and are the first cells to express *myod*. Tbxta and Tbx16 have similar DNA binding recognition sequences (Garnett et al., 2009; Nelson et al., 2017). Congruently, we find a prominent Tbxta ChIP-seq peak at the 5DE -80 kb site upstream of *myf5*, and minor peaks at the proximal sites (Fig. 6A,B; Table S3). Because of the role of Tbx16 and Tbxta in *myod* expression we also examined the *myod* locus for Tbx protein binding. We found multiple sites occupied by Tbxta and Tbx16 either individually or in combination (Table S3). Notably, only one site (DDE3) displayed strongly significant H3K4me1 and H3K27ac peaks and this was only occupied by Tbxta and not by Tbx16 (Fig. S5 and Table S3). However, an additional site (DDE1) showed significant occupancy by Tbx16 and Tbxta concurrent with H3K4me1 but not H3K27ac (Fig. S5; Table S3). In spite of the absence of a significant H3K27ac mark, this peak may be important to Tbx16 regulation of *myod*.

bioRxiv preprint doi: https://doi.org/10.1101/766501; this version posted September 12, 2019. The copyright holder for this preprint (which was not certified by peer review) is the author/funder, who has granted bioRxiv a license to display the preprint in perpetuity. It is made available under aCC-BY-NC-ND 4.0 International license.

These findings indicate that differential direct binding of Tbxta and Tbx16 may control both *myf5* and *myod* expression at the inception of skeletal myogenesis.

Is Tbxta also required for MRF expression in response to Fgf? Over-expression of Fgf4 in *tbxta* mutants successfully induced *myf5* mRNA and suppressed *aplnrb* mRNA widely in the posterior mesoderm except in a widened dorsal midline region, showing that the introduced Fgf4 was active (Fig. 7A,B). However, *myod* expression was not rescued in *tbxta* mutants in the dorsal pre-adaxial region of Fgf4-injected embryos, or elsewhere around the germ ring (Fig. 7A). Moreover, even an increased dose of 225 pg *fgf4* mRNA/embryo failed to rescue *myod* mRNA in *tbxta* mutants. Importantly, *tbxta* heterozygotes showed significantly less extensive induction of *myod* mRNA in response to Fgf4 than did their wt siblings ($p=0.0001$ X^2-test; Fig. 7C and Table S4). Therefore, Tbxta is essential for *myod* induction in pre-adaxial cells independent of its role in promoting expression of midline Fgfs.

Although Fgf4-injection did not radically alter the location of *tbx16* or *tbxta* mRNA (Fig. 5B), we noticed that the higher level of *tbx16* mRNA in adaxial compared to paraxial cells was not obvious in Fgf4-injected wt embryos, with high levels present at all dorsoventral locations, presumably because pre-adaxial character was induced widely in posterior mesoderm (Fig. 5B). Nevertheless, as Fgf4-injection into *tbxta* mutants induced *myf5* but not *myod* mRNA (Fig. 7A), it seems Tbxta is essential to progress from *myf5* to *myod* expression.

Two hypotheses could explain the lack of *myod* expression in Fgf4-injected *tbxta* mutants. First, despite the apparent lack of Tbxta protein in adaxial cells (Ochi et al., 2008; Schulte-Merker et al., 1994a), Tbxta might act directly on *myod*. Alternatively, Fgf-driven Tbxta activity might act indirectly in pre-adaxial cells to upregulate Tbx16 and thereby drive *myod* expression. We therefore examined the ability of Fgf4 to upregulate Tbx16 in *tbxta* mutants. Fgf4 enhanced *tbx16* mRNA throughout the posterior mesoderm in siblings, with the exception of the widened notochordal tissue that contained nuclear Tbxta protein and failed to upregulate MRFs (Figs 7D, 8D). In *tbxta* mutants, Fgf4 also enhanced *tbx16* mRNA in the ventral mesoderm, but a broader dorsal region did not express *tbx16*. Moreover, the level of *tbx16* mRNA appeared lower than in siblings (Fig. 7D). Thus, Fgf4-injected *tbxta* mutants lack both Tbxta and Tbx16 upregulation in pre-adaxial cells. We conclude that Fgf-driven induction of lateral myogenic tissue requires Tbx16, but not Tbxta. In contrast, induction of pre-adaxial character, marked by upregulated *myf5* and

bioRxiv preprint doi: https://doi.org/10.1101/766501; this version posted September 12, 2019. The copyright holder for this preprint (which was not certified by peer review) is the author/funder, who has granted bioRxiv a license to display the preprint in perpetuity. It is made available under aCC-BY-NC-ND 4.0 International license.

418 *myod* mRNAs, requires both Tbx genes.

419

420 ***Fgf action on Tbx16 suppresses dorsoposterior axial fate***

421 Finally, we examined the wider effect of Fgf signalling when skeletal muscle cannot form in
422 the absence of *tbx16* function. Excess Fgf action in embryos causes gross patterning
423 defects (Kimelman and Kirschner, 1987; Slack et al., 1987). When Fgf4 was over-
424 expressed in *tbx16* heterozygote in-cross lays, some anterior mesodermal tissue formed
425 and head tissues such as eye and brain were apparent, but trunk and tail mesoderm was
426 grossly deficient (Fig. 8A). In siblings over-expressing Fgf4, some muscle was formed and
427 truncated embryos were observed to twitch at 24 hpf. In contrast, no muscle was detected
428 in *tbx16* mutants (Fig. 8B). Moreover, the residual expression of mutant *tbx16* mRNA at
429 90% epiboly observed in un-injected embryos was lost upon Fgf4 over-expression (Fig.
430 8C). This suggests that the cells with tailbud character normally accumulating in *tbx16*
431 mutants were missing. Instead, widespread expression of Tbxta protein in nuclei far from
432 the germ ring suggested that the entire posterior (but not anterior) mesoderm had
433 converted to notochord, the most dorsal posterior mesoderm fate (Fig. 8D). Indeed, *shha*
434 mRNA, a marker of notochord, was found to be broadly upregulated around the embryo in
435 *tbx16* mutant embryos injected with Fgf4 mRNA, but not in their siblings (Fig. 8E). The
436 data suggest that Fgf4 drives early involution of all posterior mesoderm precursors, leaving
437 none to form a tailbud. In the presence of Tbx16, Fgf4 also dorsalizes most involuted
438 mesoderm to muscle, whereas, in the absence of Tbx16, Fgf4 converts most of the
439 mesoderm to notochord.

440

441 **Discussion**

442 The current work contains four main findings. First, that Tbx16 directly binds and activates
443 *myf5* regulatory elements to initiate skeletal myogenesis. Second, that Fgf signalling acts
444 through Tbx16 to drive the initial myogenic events in the adaxial cell lineage that
445 subsequently require Hh signalling to complete myogenesis. Third, that Tbxta, the dorsal-
446 most/posterior Tbx factor, binds directly to *myod* regulatory elements and also promotes
447 dorsal midline expression of Fgfs that subsequently cooperate to drive dorsal myogenesis
448 through Tbx16. Fourth, that Fgf action through Tbx16 suppresses the dorsoposterior axial
449 fate induced by Tbxta. Overall, Tbx transcription factors provide a crucial link between

bioRxiv preprint doi: https://doi.org/10.1101/766501; this version posted September 12, 2019. The copyright holder for this preprint (which was not certified by peer review) is the author/funder, who has granted bioRxiv a license to display the preprint in perpetuity. It is made available under aCC-BY-NC-ND 4.0 International license.

mesoderm induction and the initiation of myogenesis, which has profound implications for understanding the evolution of vertebrates.

Tbx genes and myogenesis

Building on previous evidence that Tbx16 up-regulates *myf5* mRNA level (Garnett et al., 2009; Mueller et al., 2010), our findings that Tbx16 protein binds to DNA elements near the *myf5* and *myod* genes, is required for their expression, and can induce them in the absence of protein synthesis show that these MRF genes are direct targets of Tbx16. We also present evidence that *myf5* and *myod* are direct targets of Tbxta, including the presence of several significant Tbxta ChIP-seq peaks and the requirement for Tbxta to transduce Fgf4-mediated signalling into *myod* expression. As MRF gene activity, principally that of *myf5* and *myod*, drives commitment to skeletal myogenesis in vertebrates, our findings place Tbx protein activity at the base of skeletal myogenesis in zebrafish.

Before myogenesis, Tbx16 is required for migration of most trunk PSM cells away from the 'maturation zone' immediately after their involution (Griffin and Kimelman, 2002; Row et al., 2011). Our analysis of *aplnrb*-expressing mesodermal cells shows that most anterior (i.e. head) and posterior ventral (i.e. ventral trunk) mesoderm involution and migration occurs normally in both *tbx16* and *tbxta* mutants. Indeed, some PSM is formed in *tbx16* mutants and goes on to make small amounts of muscle (Amacher et al., 2002; Kimmel et al., 1989). PSM formation is more severely lacking in *tbx16;tbxta* or *tbx16;tbx16l* double mutants (Amacher et al., 2002; Griffin et al., 1998; Morrow et al., 2017; Nelson et al., 2017) or after knockdown of Tbxtb in *tbxta* mutant (Martin and Kimelman, 2008). Cooperation of Tbx proteins in PSM formation also occurs in *Xenopus tropicalis* (Gentsch et al., 2013). It is likely, therefore, that all PSM formation and its accompanying *myf5* expression requires Tbx proteins. Our findings also help to explain the observation that *tbx16* mutants have increased pronephric mesoderm (Warga et al., 2013). As Tbx16 is required for direct induction of *myf5* and for *pcdh8, msgn1, mespaa* and *tbx6* expression in PSM (Fior et al., 2012; Goering et al., 2003; Griffin and Kimelman, 2002; Lee et al., 2009; Morrow et al., 2017; Yamamoto et al., 1998), the data support previous proposals (Amacher and Kimmel, 1998; Griffin and Kimelman, 2002) of a role for Tbx16 in promotion of the earliest step in PSM formation, *en route* to myogenesis. These early actions of Tbx16 and Tbxta proteins have previously masked their direct myogenic actions in mutants.

bioRxiv preprint doi: https://doi.org/10.1101/766501; this version posted September 12, 2019. The copyright holder for this preprint (which was not certified by peer review) is the author/funder, who has granted bioRxiv a license to display the preprint in perpetuity. It is made available under aCC-BY-NC-ND 4.0 International license.

To identify likely MRF enhancers at 80% epiboly, we have largely restricted our focus to robust Tbx16 and Tbxta ChIP-seq peaks that are co-incident with established histone marks indicative of active enhancers, H3K4me1 and H3K27ac. This approach is driven by the accepted knowledge that most transcription factor binding events are unlikely to be functionally important, and the availability of stage-matched ChIP-seq data for these established histone marks (Bogdanovic et al., 2012). However, there is an increasing realization that comprehensive identification of enhancers will require a more complete analysis of further histone acetylation events, as evidenced by the recent discovery of functional enhancers marked by H3K122ac, H3K64ac and/or H4K16ac, many of which lack H3K27ac (Pradeepa, 2017; Pradeepa et al., 2016). It is therefore possible that additional Tbx16 and Tbxta ChIP-seq peaks beyond 5DE, 5PE1 and DDE3 may mark functionally important enhancers regulating *myf5* and *myod*. Of particular note is DDE1, -31kb upstream of *myod*, which is colocalized with a significant H3K4me1 mark, though not H3K27ac. Given that *myod* expression is restricted to a minor cell population at 80% epiboly, we further note that the probability of detecting significant histone marks specific to this population is low due to averaging of signal across whole embryos. It is therefore possible that the ChIP-seq peak common to Tbx16 and Tbxta at the DDE1 -31kb upstream of *myod* is functionally important. Given that Tbx16 is essential for *myod* expression in pre-adaxial cells and can upregulate *myod* in the absence of protein synthesis, this ChIP-seq peak may represent a key region mediating this direct transcriptional activation. Our data argue that once posterior (i.e. trunk) mesoderm forms, Tbx proteins are still required for MRF expression and normal myogenesis. Hh signalling from notochord acts to maintain adaxial MRF expression in wild type and, if Tbx-driven initiation fails, Hh can initiate *myod* and up-regulate *myf5* expression, thereby driving slow myogenesis (Blagden et al., 1997; Coutelle et al., 2001; Du et al., 1997). When Hh signalling is prevented, the small amount of trunk PSM that forms in *tbx16* mutants activates low level *myf5* but not *myod* mRNA expression, showing that Tbx16 is essential for initial pre-adaxial *myod* transcription. *Tbxta* mutants also fail to initiate pre-adaxial *myod* expression. Conversely, overexpression of Tbx16 directly induces ectopic *myf5* mRNA, but only in mesoderm and preferentially in dorsal mesoderm at somite levels. In contrast, Tbx16-induced ectopic *myod* expression is restricted to a narrower mesodermal region flanking the pre-adaxial cells, likely due to the restricted expression of *smarcd3* in this region (Ochi et al., 2008). Nevertheless, *myod* is induced by Tbx16 in the absence of Myf5, probably through direct binding to regulatory elements in the *myod* locus. It is thus likely that changes in

bioRxiv preprint doi: https://doi.org/10.1101/766501; this version posted September 12, 2019. The copyright holder for this preprint (which was not certified by peer review) is the author/funder, who has granted bioRxiv a license to display the preprint in perpetuity. It is made available under aCC-BY-NC-ND 4.0 International license.

chromatin structure in the *myf5* and *myod* loci that accompany posterior mesoderm formation facilitate Tbx16 access to its binding sites in these MRF genes.

In considering the role of Tbx genes in myogenesis it is essential to distinguish adaxial and paraxial myogenesis, which give rise to different kinds of muscle with distinct timing (Blagden et al., 1997; Devoto et al., 1996). Paraxial PSM cells form fast muscle after somitogenesis. As posterior mesoderm involutes during gastrulation, *myf5* expression is initiated throughout the PSM. Tbx16, but not Tbxta, is required for almost all this low level *myf5* expression. In wild type, *myf5* mRNA then declines as paraxial PSM matures before being up-regulated once more as somite borders form (Coutelle et al., 2001). In contrast, pre-adaxial cells require both Tbxta and Tbx16 function for up-regulation of *myf5* and initiation of *myod* expression, and then commence terminal differentiation within the PSM to generate slow muscle. Thus, distinct Tbx proteins are required for normal adaxial and paraxial myogenesis.

Our data show that Tbx16 is a key direct regulator of MRFs required for myogenesis. The expression of low levels of *myf5* mRNA and formation of small amounts of both fast and slow muscle in the trunk and more in the tail in *tbx16* mutants are likely driven by Tbx16l (formerly known as Tbx6 and then Tbx6l) (Morrow et al., 2017). Morrow et al (2017) show that tail somite formation is prevented and tail *myod* mRNA diminished in the *tbx16;tbx16l* double mutant, but that *myod* mRNA expression continues at a reduced level throughout the axis at 24 hpf. Our data argue that the residual *myod* mRNA is in adaxially-derived slow muscle induced by Hh signalling.

Other Tbx proteins may directly regulate myogenic initiation in other body regions and species, as many Tbx proteins bind similar DNA motifs (Papaioannou, 2014). For example, Tbx1, Tbx5a and Tbx20 are required in anterior mesoderm for patterning of cranial and cardiac muscles (Knight et al., 2008; Lu et al., 2017; Valasek et al., 2011). *Tbx4/5a* gene function is required for limb muscle patterning, at least partially non-cell autonomously (Don et al., 2016; Hasson et al., 2010; Valasek et al., 2011). Tbx6 suppresses myogenesis in anterior PSM indirectly through Mesp-b (Windner et al., 2015), but direct actions of Tbx6 could also regulate myogenesis. The increasing complexity of Tbx gene diversity during vertebrate evolution may have permitted muscle diversification.

Fgf and myogenesis

bioRxiv preprint doi: https://doi.org/10.1101/766501; this version posted September 12, 2019. The copyright holder for this preprint (which was not certified by peer review) is the author/funder, who has granted bioRxiv a license to display the preprint in perpetuity. It is made available under aCC-BY-NC-ND 4.0 International license.

Tbx16 is required for Fgf signalling to induce *myf5* (Fig. 5A). In its absence, Fgf drives all posterior mesoderm to a notochord-like fate (Fig. 8D,E), probably via activation of Tbxta. It has long been known that Fgf signalling is required for expression of *myf5* in the paraxial PSM of the tailbud (Groves et al., 2005). Here we show Fgf is also required for the earliest *myf5* expression in invaginating trunk mesoderm and for the initiation of *myf5* and *myod* expression in pre-adaxial cells destined to form the slow muscle of anterior somites. Our data also extend the evidence that this MRF expression is subsequently maintained, as the shield/tailbud-derived sources of Fgf recede from the adaxial cells, by Hh signalling from the maturing notochord (Coutelle et al., 2001; Osborn et al., 2011). The finding that the latter Fgf action is restricted to trunk (as opposed to tail) somites is consistent with a) the dwindling level of Fgf mRNAs in the chordoneural hinge as tailbud outgrowth slows becoming insufficient to promote MRF expression and b) the unresolved issue of Hh-independent initiation of MRF expression in the anteriormost somites of murine *smoothened* mutants (Zhang et al., 2001). We suggest this MRF expression is Fgf-triggered in mouse, as in zebrafish.

Tbxta is also required for normal Fgf signalling from the midline to promote pre-adaxial myogenesis. One likely reason is the loss of *fgf4, fgf6a*, *fgf8a, fgf8b* and possibly *fgf3* expression in the dorsal midline chordoneural hinge region in *tbxta* mutants (Fig. 3B)(Draper et al., 2003). When Fgf4 or Fgf6a is artificially over-expressed in *tbxta* mutants, *myf5* is readily induced. This suggests that Tbxta protein is not required cell autonomously to drive *myf5* expression, even though our data reveal that Tbxta binds in vivo to similar regions of the *myf5* locus to those bound by Tbx16. In marked contrast, Tbxta is essential for over-expressed Fgf to induce *myod*. Interestingly, ChIP shows Tbxta binding sites upstream of *myod* that are preferentially bound by Tbtxa, suggesting that Tbxta binding to one or more of these sites directly activates *myod* in response to Fgf. We note, however, that Tbxta protein is immunodetectable in notochord and germ ring cells but barely in *myod*-expressing pre-adaxial cells (Hammerschmidt and Nüsslein-Volhard, 1993; Odenthal et al., 1996; Schulte-Merker et al., 1994a). Nevertheless, as pre-adaxial cells have recently expressed Tbxta during their involution, it is possible that functionally significant protein could remain bound at the *myod* locus. Transient persistence of Tbxta is consistent with the downregulation of *myod* mRNA in more anterior adaxial cells in the absence of Hh signals. An alternative hypothesis of indirect regulation of *myod* by Fgf through another transcription factor, such as Tbx16, is also tenable, and is supported by

bioRxiv preprint doi: https://doi.org/10.1101/766501; this version posted September 12, 2019. The copyright holder for this preprint (which was not certified by peer review) is the author/funder, who has granted bioRxiv a license to display the preprint in perpetuity. It is made available under aCC-BY-NC-ND 4.0 International license.

582 the reduced upregulation of *tbx16* observed in *tbxta* mutants injected with Fgf4 (Fig. 7D).
583 We show that Myf5 is not an indirect mediator of Fgf signalling on *myod*, despite its Fgf
584 sensitivity.

585 Our data argue strongly that Fgf signalling not only promotes *tbx16* expression, but also
586 enhances the activity of the Tbx16 protein. The MRF inducing activity of Tbx16 is
587 suppressed by inhibition of Fgf signalling (Fig. 5C,D). Bearing in mind the existence of
588 Tbx16l and Tbxta, this result is consistent with the finding that *tbxta* or *tbx16* mutation
589 sensitizes embryos to Fgf inhibition (Griffin and Kimelman, 2003). As Tbx16
590 overexpression can expand PSM fates and reverse the effect of partial Fgf inhibition, a
591 primary role of Fgf signalling is to cooperate with Tbx16 to drive expression of its target
592 genes, including *myf5*. This understanding provides mechanistic insight into how the
593 effects of Fgf on gastrulation movements and histogenesis are separated, as originally
594 proposed (Amaya et al., 1993). Interestingly, Tbx16 over-expression rescues *myf5* mRNA
595 preferentially on the dorsal side of the embryo, suggesting that BMP and/or other signals
596 continue to suppress PSM fates ventrally, and thus that Tbx16 does not act by simply
597 suppressing the inhibitory effect of such signals.

598 We find that in the absence of Tbxta, Fgf acts to induce Tbx16 in ventral regions (Fig. 7D).
599 The data are fully consistent with a positive feedback loop between Tbxta and Fgf
600 signalling to maintain tailbud character and notochord formation. Additionally, our findings
601 suggest that Tbx16 acts in competition with Tbxta to suppress tailbud/notochord fate and
602 Fgf expression and to promote paraxial fates. Ochi et al. (2008) have suggested Tbxta
603 and Fgf work through Smarcd3 (Baf60c) to permit pre-adaxial cell formation. It is striking
604 that the requirement for both Tbxta and Tbx16 proteins to generate adaxial cells located
605 between the axial and paraxial regions triggers the first step of diversification of muscle to
606 slow and fast contractile character.

607

608 ***Evolution of vertebrates***

609 From an evolutionary perspective, our findings yield a number of important insights. As
610 efficient motility is a key feature of animals, and efficient sarcomeric muscle is found
611 throughout triploblasts, it is likely that mesodermal striated muscle existed in the common
612 ancestor of deuterostomes and protostomes. It is widely thought that chordates evolved
613 from an early deuterostome consisting of a segmented 'branchial basket', possibly

bioRxiv preprint doi: https://doi.org/10.1101/766501; this version posted September 12, 2019. The copyright holder for this preprint (which was not certified by peer review) is the author/funder, who has granted bioRxiv a license to display the preprint in perpetuity. It is made available under aCC-BY-NC-ND 4.0 International license.

attached to a propulsive segmented pre-anal trunk. There is consensus that subsequent appearance of neural crest, notochord and a post-anal tail were significant evolutionary steps for chordates (Gee, 2018). Already in cephalochordates at least two kinds of striated muscle had evolved in anterior somites (Devoto et al., 2006; Lacalli, 2002). Our evidence that initiation of both slow and fast myogenesis in the most anterior trunk is driven by Fgf/Tbx signalling indicates that a major function of this early mesodermal inducer was induction of trunk striated myogenesis, which may constitute an ancestral chordate character. Once Hh is expressed in maturing midline tissues, it triggers terminal differentiation of muscle precursors into functional muscle through a positive feedback loop (Coutelle et al., 2001; Osborn et al., 2011). Parallel diversification of neural tube cells, also regulated by Hh (Placzek and Briscoe, 2018), may have generated matching motoneural and muscle fibre populations that enhanced organismal motility. With the evolution of a *tbxta*-dependent tailbud destined to make the post-anal tail, our data suggest that weakening Fgf signalling continued to induce *myf5* expression and paraxial mesoderm character through *tbx16*, but was insufficient to induce adaxial myogenesis. The presence of Hh and Tbxta plus Tbx16, however, ensure that adaxial slow muscle is initiated in the zebrafish tail.

In the anterior somites of amniotes, as in zebrafish, Hh signalling maintains, rather than initiates *myf5* expression (Zhang et al., 2001). In more posterior somites of zebrafish, Xenopus and amniote, Hh signalling drives *myf5* initiation (Borycki et al., 1999; Grimaldi et al., 2004). Compared to zebrafish, however, murine *Myf5* induction is further delayed until after somitogenesis, when Gli3 repressive signals in PSM have diminished (McDermott et al., 2005). In mouse, Brachyury/Tbxt is required for myogenesis and binds 20 kb downstream of *Myod*, but does not obviously control its expression (Lolas et al., 2014). No clear orthologue of *tbx16* exists in mammals, although it clusters by sequence with *Tbx6* genes. In mammals, Tbx6 suppresses neurogenesis in posterior paraxial mesoderm, suggesting that additional mechanisms have evolved that suppress early pre-somitic *Myf5* expression (Chapman and Papaioannou, 1998). Indeed, possible low level *Myf5* expression in PSM has long been a source of controversy (George-Weinstein et al., 1996; Gerhart et al., 2004). Thus, there has been diversification in how these Tbx genes regulate somitic myogenesis.

Our data suggest that regions required for *myf5* expression are located ~80 kb upstream of the transcription start site. A BAC transgenic encompassing 80 kb upstream and 76 kb

bioRxiv preprint doi: https://doi.org/10.1101/766501; this version posted September 12, 2019. The copyright holder for this preprint (which was not certified by peer review) is the author/funder, who has granted bioRxiv a license to display the preprint in perpetuity. It is made available under aCC-BY-NC-ND 4.0 International license.

downstream of *myf5* has been shown to drive GFP expression in muscle (Chen et al., 2007). However, analysis of shorter constructs has been confounded by cloning artefacts (Chen et al., 2001; Chen et al., 2007), leaving understanding of elements driving specific aspects of zebrafish *myf5* expression unclear. Murine *Myf5* is also regulated by many distant elements (Buckingham and Rigby, 2014). Similarly, we observe Tbx binding peaks far upstream of zebrafish *myod*. Upstream elements are known to initiate murine *Myod* expression in some embryonic regions, but whether these elements drive the earliest myotomal regulation of *Myod* is unknown (Chen and Goldhamer, 2004). The extent to which similar transcription factors act through similar binding elements to initiate MRF expression and myogenesis across vertebrates remains to be determined.

The ancestral situation seems clearer. In amphioxus, *Tbx6/16* is expressed in tailbud and PSM (Belgacem et al., 2011). In *Ciona*, knockdown of Tbx6b/c/d leads to reduced *MyoD* expression, loss of muscle and paralysis (Imai et al., 2006). In *Xenopus*, both Tbx6 and VegT are implicated in early myogenesis (Callery et al., 2010; Fukuda et al., 2010; Tazumi et al., 2010), although some mechanisms may differ from those in zebrafish (Maguire et al., 2012). By adding our zebrafish findings, we show that in all major chordate groups Tbx-dependent gene regulation is central to skeletal myogenesis. The conserved involvement, yet divergent detail, of how *Tbx16*, *Tbx6* and *Tbxt* genes regulate somitic myogenic diversity along the body axis are consistent with selective pressures on these duplicated Tbx gene families playing a key role in the diversification of myogenesis in the vertebrate trunk and tail, characters that gave chordates their predatory advantage.

bioRxiv preprint doi: https://doi.org/10.1101/766501; this version posted September 12, 2019. The copyright holder for this preprint (which was not certified by peer review) is the author/funder, who has granted bioRxiv a license to display the preprint in perpetuity. It is made available under aCC-BY-NC-ND 4.0 International license.

Materials and methods

Zebrafish lines and maintenance

Mutant lines *fgf8a*^{ti282a} (Reifers et al., 1998), *noto*^{n1} (Talbot et al., 1995), *smo*^{b641} (Barresi et al., 2000), *tbxta*^{b195} and *tbx16*^{b104} (Griffin et al., 1998) are likely nulls and were maintained on King's wild type background. Staging and husbandry were as described previously (Westerfield, 2000). All experiments were performed under licences awarded under the UK Animal (Scientific Procedures) Act 1986 and subsequent modifications.

In situ mRNA hybridization and immunohistochemistry

In situ mRNA hybridization for *myf5* and *myod* was as described previously (Hinits et al., 2009). Additional probes were *fgf3* (Maroon et al., 2002), *fgf4* (IMAGE: 6790533), *fgf6*a (Thisse and Thisse, 2005), *fgf8a* (Reifers et al., 1998), *tbxta* (Schulte-Merker et al., 1994b) and *tbx16* (Griffin et al., 1998; Ruvinsky et al., 1998). Anti-Ntla immunostaining was performed after in situ hybridization using rabbit anti-Ntla (Schulte-Merker et al., 1992, 1:2000) and Horse anti-rabbit IgG-HRP conjugated (Vector Laboratories, Inc.)

Embryo Manipulations

Embryos were injected with MOs (GeneTools LLC) as indicated in Table S2 to *fgf3*, *fgf4*, *fgf6a*, *fgf8a*, *tbxta* (Feldman and Stemple, 2001) or *tbx16* (Bisgrove et al., 2005). Controls were vehicle or irrelevant mismatch MO. Cyclopamine (100 μM in embryo medium), SU5402 (at indicted concentration in embryo medium) and vehicle control were added at 30% epiboly to embryos whose chorions had been punctured with a 30G hypodermic needle. A PCR product of *fgf4* (IMAGE: 6790533) was cloned (primers in Table S2) into the SacI/SalI sites of pßUT3 to make mRNA for over-expression. 100-220 pg *fgf4* mRNA (made with messageMachine), 50 pg *fgf6a* mRNA, 150 pg *tbx16* mRNA (Griffin et al., 1998) or 150 pg *tbx16*-GR mRNA (Jahangiri et al., 2012) were injected into 1-cell-stage embryos. For hormone-inducible Tbx16 activation, embryos were treated with 10 μg/ml final concentration of cycloheximide two hours prior to collection at 75-80% epiboly. After 30 min, 20 μM dexamethasone was added for the remaining 1.5 h.

Chromatin immunoprecipitation and sequencing (ChIP-seq) and ChIP-qPCR

bioRxiv preprint doi: https://doi.org/10.1101/766501; this version posted September 12, 2019. The copyright holder for this preprint (which was not certified by peer review) is the author/funder, who has granted bioRxiv a license to display the preprint in perpetuity. It is made available under aCC-BY-NC-ND 4.0 International license.

ChIP-seq data was analysed as reported previously (Nelson et al., 2017). ChIP-qPCR experiments were performed as previously reported (Jahangiri et al., 2012) using the primers in Table S2.

Acknowledgements

We are grateful to all members of the Hughes lab for advice and to Bruno Correia da Silva and his staff for care of the fish. SMH is an MRC Scientist with MRC Programme Grant (G1001029 and MR/N021231/1) support. This work was also supported by grants from the British Heart Foundation to YH and SMH (PG PG/14/12/30664) and to FCW (PG/13/19/30059).

References

Amacher, S.L., Draper, B.W., Summers, B.R., Kimmel, C.B., 2002. The zebrafish T-box genes no tail and spadetail are required for development of trunk and tail mesoderm and medial floor plate. Development 129, 3311-3323.

Amacher, S.L., Kimmel, C.B., 1998. Promoting notochord fate and repressing muscle development in zebrafish axial mesoderm. Development 125, 1397-1406.

Amack, J.D., Wang, X., Yost, H.J., 2007. Two T-box genes play independent and cooperative roles to regulate morphogenesis of ciliated Kupffer's vesicle in zebrafish. Dev Biol 310, 196-210.

Amaya, E., Stein, P.A., Musci, T.J., Kirschner, M.W., 1993. FGF signalling in the early specification of mesoderm in Xenopus. Development 118, 477-487.

Arenas-Mena, C., 2013. Brachyury, Tbx2/3 and sall expression during embryogenesis of the indirectly developing polychaete Hydroides elegans. The International journal of developmental biology 57, 73-83.

Barresi, M.J., Stickney, H.L., Devoto, S.H., 2000. The zebrafish slow-muscle-omitted gene product is required for Hedgehog signal transduction and the development of slow muscle identity. Development 127, 2189-2199.

Beattie, C.E., Hatta, K., Halpern, M.E., Liu, H., Eisen, J.S., Kimmel, C.B., 1997. Temporal separation in the specification of primary and secondary motoneurons in zebrafish. Dev Biol 187, 171-182.

Belgacem, M.R., Escande, M.L., Escriva, H., Bertrand, S., 2011. Amphioxus Tbx6/16 and Tbx20 embryonic expression patterns reveal ancestral functions in chordates. Gene Expr Patterns 11, 239-243.

Bisgrove, B.W., Snarr, B.S., Emrazian, A., Yost, H.J., 2005. Polaris and Polycystin-2 in dorsal forerunner cells and Kupffer's vesicle are required for specification of the zebrafish left-right axis. Dev Biol 287, 274-288.

Blagden, C.S., Currie, P.D., Ingham, P.W., Hughes, S.M., 1997. Notochord induction of zebrafish slow muscle mediated by Sonic Hedgehog. Genes Dev 11, 2163-2175.

Bogdanovic, O., Fernandez-Minan, A., Tena, J.J., de la Calle-Mustienes, E., Hidalgo, C., van Kruysbergen, I., van Heeringen, S.J., Veenstra, G.J., Gomez-Skarmeta, J.L., 2012. Dynamics of enhancer chromatin signatures mark the transition from pluripotency to cell specification during embryogenesis. Genome research 22, 2043-2053.

bioRxiv preprint doi: https://doi.org/10.1101/766501; this version posted September 12, 2019. The copyright holder for this preprint (which was not certified by peer review) is the author/funder, who has granted bioRxiv a license to display the preprint in perpetuity. It is made available under aCC-BY-NC-ND 4.0 International license.

746 Borycki, A.G., Brunk, B., Tajbakhsh, S., Buckingham, M., Chiang, C., Emerson, C.P., Jr.,
747 1999. Sonic hedgehog controls epaxial muscle determination through Myf5 activation.
748 Development 126, 4053-4063.
749 Bouldin, C.M., Manning, A.J., Peng, Y.H., Farr, G.H., 3rd, Hung, K.L., Dong, A., Kimelman,
750 D., 2015. Wnt signaling and tbx16 form a bistable switch to commit bipotential
751 progenitors to mesoderm. Development 142, 2499-2507.
752 Brunet, T., Lauri, A., Arendt, D., 2015. Did the notochord evolve from an ancient axial
753 muscle? The axochord hypothesis. Bioessays 37, 836-850.
754 Buckingham, M., Rigby, P.W., 2014. Gene regulatory networks and transcriptional
755 mechanisms that control myogenesis. Dev Cell 28, 225-238.
756 Callery, E.M., Thomsen, G.H., Smith, J.C., 2010. A divergent Tbx6-related gene and Tbx6
757 are both required for neural crest and intermediate mesoderm development in
758 Xenopus. Dev Biol 340, 75-87.
759 Chapman, D.L., Papaioannou, V.E., 1998. Three neural tubes in mouse embryos with
760 mutations in the T-box gene Tbx6. Nature 391, 695-697.
761 Chen, J.C., Goldhamer, D.J., 2004. The core enhancer is essential for proper timing of
762 MyoD activation in limb buds and branchial arches. Dev Biol 265, 502-512.
763 Chen, Y.H., Lee, W.C., Liu, C.F., Tsai, H.J., 2001. Molecular structure, dynamic
764 expression, and promoter analysis of zebrafish (Danio rerio) myf-5 gene. Genesis 29,
765 22-35.
766 Chen, Y.H., Wang, Y.H., Chang, M.Y., Lin, C.Y., Weng, C.W., Westerfield, M., Tsai, H.J.,
767 2007. Multiple upstream modules regulate zebrafish myf5 expression. BMC
768 developmental biology 7, 1.
769 Chiba, S., Jiang, D., Satoh, N., Smith, W.C., 2009. Brachyury null mutant-induced defects
770 in juvenile ascidian endodermal organs. Development 136, 35-39.
771 Coutelle, O., Blagden, C.S., Hampson, R., Halai, C., Rigby, P.W., Hughes, S.M., 2001.
772 Hedgehog signalling is required for maintenance of myf5 and myoD expression and
773 timely terminal differentiation in zebrafish adaxial myogenesis. Dev Biol 236, 136-150.
774 Devoto, S.H., Melancon, E., Eisen, J.S., Westerfield, M., 1996. Identification of separate
775 slow and fast muscle precursor cells in vivo, prior to somite formation. Development
776 122, 3371-3380.
777 Devoto, S.H., Stoiber, W., Hammond, C.L., Steinbacher, P., Haslett, J.R., Barresi, M.J.,
778 Patterson, S.E., Adiarte, E.G., Hughes, S.M., 2006. Generality of vertebrate
779 developmental patterns: evidence for a dermomyotome in fish. Evol Dev 8, 101-110.
780 Dietrich, S., Schubert, F.R., Gruss, P., Lumsden, A., 1999. The role of the notochord for
781 epaxial myotome formation in the mouse. Cell Mol Biol (Noisy-le-grand) 45, 601-616.
782 Don, E.K., de Jong-Curtain, T.A., Doggett, K., Hall, T.E., Heng, B., Badrock, A.P., Winnick,
783 C., Nicholson, G.A., Guillemin, G.J., Currie, P.D., Hesselson, D., Heath, J.K., Cole,
784 N.J., 2016. Genetic basis of hindlimb loss in a naturally occurring vertebrate model.
785 Biology open 5, 359-366.
786 Draper, B.W., Stock, D.W., Kimmel, C.B., 2003. Zebrafish fgf24 functions with fgf8 to
787 promote posterior mesodermal development. Development 130, 4639-4654.
788 Du, S.J., Devoto, S.H., Westerfield, M., Moon, R.T., 1997. Positive and negative regulation
789 of muscle cell identity by members of the *hedgehog* and *TGF-b* gene families. Journal
790 of Cell Biology 139, 145-156.
791 Feldman, B., Stemple, D.L., 2001. Morpholino phenocopies of sqt, oep, and ntl mutations.
792 Genesis 30, 175-177.
793 Fior, R., Maxwell, A.A., Ma, T.P., Vezzaro, A., Moens, C.B., Amacher, S.L., Lewis, J.,
794 Saude, L., 2012. The differentiation and movement of presomitic mesoderm progenitor
795 cells are controlled by Mesogenin 1. Development 139, 4656-4665.

bioRxiv preprint doi: https://doi.org/10.1101/766501; this version posted September 12, 2019. The copyright holder for this preprint (which was not certified by peer review) is the author/funder, who has granted bioRxiv a license to display the preprint in perpetuity. It is made available under aCC-BY-NC-ND 4.0 International license.

796 Fukuda, M., Takahashi, S., Haramoto, Y., Onuma, Y., Kim, Y.J., Yeo, C.Y., Ishiura, S.,
797 Asashima, M., 2010. Zygotic VegT is required for Xenopus paraxial mesoderm
798 formation and is regulated by Nodal signaling and Eomesodermin. The International
799 journal of developmental biology 54, 81-92.
800 Furthauer, M., Reifers, F., Brand, M., Thisse, B., Thisse, C., 2001. sprouty4 acts in vivo as
801 a feedback-induced antagonist of FGF signaling in zebrafish. Development 128, 2175-
802 2186.
803 Garnett, A.T., Han, T.M., Gilchrist, M.J., Smith, J.C., Eisen, M.B., Wardle, F.C., Amacher,
804 S.L., 2009. Identification of direct T-box target genes in the developing zebrafish
805 mesoderm. Development 136, 749-760.
806 Gee, H., 2018. Across the Bridge: Understanding the Origin of the Vertebrates. The
807 University of Chicago Press, London.
808 Gentsch, G.E., Owens, N.D., Martin, S.R., Piccinelli, P., Faial, T., Trotter, M.W., Gilchrist,
809 M.J., Smith, J.C., 2013. In vivo T-box transcription factor profiling reveals joint
810 regulation of embryonic neuromesodermal bipotency. Cell reports 4, 1185-1196.
811 George-Weinstein, M., Gerhart, J., Reed, R., Flynn, J., Callihan, B., Mattiacci, M., Miehle,
812 C., Foti, G., Lash, J.W., Weintraub, H., 1996. Skeletal myogenesis: the preferred
813 pathway of chick embryo epiblast cells in vitro. Dev Biol 173, 279-291.
814 Gerhart, J., 2001. Evolution of the organizer and the chordate body plan. The International
815 journal of developmental biology 45, 133-153.
816 Gerhart, J., Neely, C., Stewart, B., Perlman, J., Beckmann, D., Wallon, M., Knudsen, K.,
817 George-Weinstein, M., 2004. Epiblast cells that express MyoD recruit pluripotent cells
818 to the skeletal muscle lineage. J Cell Biol.
819 Goering, L.M., Hoshijima, K., Hug, B., Bisgrove, B., Kispert, A., Grunwald, D.J., 2003. An
820 interacting network of T-box genes directs gene expression and fate in the zebrafish
821 mesoderm. Proc Natl Acad Sci U S A 100, 9410-9415.
822 Griffin, K., Patient, R., Holder, N., 1995. Analysis of FGF function in normal and *no tail*
823 zebrafish embryos reveals separate mechanisms for formation of the trunk and tail.
824 Development 121, 2983-2994.
825 Griffin, K.J., Amacher, S.L., Kimmel, C.B., Kimelman, D., 1998. Molecular identification of
826 spadetail: regulation of zebrafish trunk and tail mesoderm formation by T-box genes.
827 Development 125, 3379-3388.
828 Griffin, K.J., Kimelman, D., 2002. One-Eyed Pinhead and Spadetail are essential for heart
829 and somite formation. Nat Cell Biol 4, 821-825.
830 Griffin, K.J., Kimelman, D., 2003. Interplay between FGF, one-eyed pinhead, and T-box
831 transcription factors during zebrafish posterior development. Dev Biol 264, 456-466.
832 Grimaldi, A., Tettamanti, G., Martin, B.L., Gaffield, W., Pownall, M.E., Hughes, S.M., 2004.
833 Hedgehog regulation of superficial slow muscle fibres in Xenopus and the evolution of
834 tetrapod trunk myogenesis. Development 131, 3249-3262.
835 Groves, J.A., Hammond, C.L., Hughes, S.M., 2005. Fgf8 drives myogenic progression of a
836 novel lateral fast muscle fibre population in zebrafish. Development 132, 4211-4222.
837 Haeussler, M., Zweig, A.S., Tyner, C., Speir, M.L., Rosenbloom, K.R., Raney, B.J., Lee,
838 C.M., Lee, B.T., Hinrichs, A.S., Gonzalez, J.N., Gibson, D., Diekhans, M., Clawson, H.,
839 Casper, J., Barber, G.P., Haussler, D., Kuhn, R.M., Kent, W.J., 2019. The UCSC
840 Genome Browser database: 2019 update. Nucleic Acids Res 47, D853-D858.
841 Halpern, M.E., Ho, R.K., Walker, C., Kimmel, C.B., 1993. Induction of muscle pioneers and
842 floor plate is distinguished by the zebrafish no tail mutation. Cell 75, 99-111.
843 Halpern, M.E., Thisse, C., Ho, R.K., Thisse, B., Riggleman, B., Trevarrow, B., Weinberg,
844 E.S., Postlethwait, J.H., Kimmel, C.B., 1995. Cell-autonomous shift from axial to

bioRxiv preprint doi: https://doi.org/10.1101/766501; this version posted September 12, 2019. The copyright holder for this preprint (which was not certified by peer review) is the author/funder, who has granted bioRxiv a license to display the preprint in perpetuity. It is made available under aCC-BY-NC-ND 4.0 International license.

paraxial mesodermal development in zebrafish floating head mutants. Development 121, 4257-4264.

Hammerschmidt, M., Nüsslein-Volhard, C., 1993. The expression of a zebrafish gene homologous to Drosophila snail suggests a conserved function in invertebrate and vertebrate gastrulation. Development 119, 1107-1118.

Hasson, P., DeLaurier, A., Bennett, M., Grigorieva, E., Naiche, L.A., Papaioannou, V.E., Mohun, T.J., Logan, M.P., 2010. Tbx4 and tbx5 acting in connective tissue are required for limb muscle and tendon patterning. Dev Cell 18, 148-156.

Hinits, Y., Osborn, D.P., Hughes, S.M., 2009. Differential requirements for myogenic regulatory factors distinguish medial and lateral somitic, cranial and fin muscle fibre populations. Development 136, 403-414.

Hinits, Y., Williams, V.C., Sweetman, D., Donn, T.M., Ma, T.P., Moens, C.B., Hughes, S.M., 2011. Defective cranial skeletal development, larval lethality and haploinsufficiency in Myod mutant zebrafish. Dev Biol 358, 102-112.

Hirsinger, E., Stellabotte, F., Devoto, S.H., Westerfield, M., 2004. Hedgehog signaling is required for commitment but not initial induction of slow muscle precursors. Dev Biol 275, 143-157.

Ho, R.K., Kane, D.A., 1990. Cell-autonomous action of zebrafish spt-1 mutation in specific mesodermal precursors. Nature 348, 728-730.

Honjo, Y., Eisen, J.S., 2005. Slow muscle regulates the pattern of trunk neural crest migration in zebrafish. Development 132, 4461-4470.

Imai, K.S., Levine, M., Satoh, N., Satou, Y., 2006. Regulatory blueprint for a chordate embryo. Science 312, 1183-1187.

Isaacs, H.V., Deconinck, A.E., Pownall, M.E., 2007. FGF4 regulates blood and muscle specification in Xenopus laevis. Biology of the cell / under the auspices of the European Cell Biology Organization 99, 165-173.

Itoh, N., Konishi, M., 2007. The zebrafish fgf family. Zebrafish 4, 179-186.

Jahangiri, L., Nelson, A.C., Wardle, F.C., 2012. A cis-regulatory module upstream of deltaC regulated by Ntla and Tbx16 drives expression in the tailbud, presomitic mesoderm and somites. Dev Biol 371, 110-120.

Kimelman, D., Kirschner, M., 1987. Synergistic induction of mesoderm by FGF and TGF-beta and the identification of an mRNA coding for FGF in the early Xenopus embryo. Cell 51, 869-877.

Kimmel, C.B., Kane, D.A., Walker, C., Warga, R.M., Rothman, M.B., 1989. A mutation that changes cell movement and cell fate in the zebrafish embryo. Nature 337, 358-362.

Kispert, A., Herrmann, B.G., Leptin, M., Reuter, R., 1994. Homologs of the mouse Brachyury gene are involved in the specification of posterior terminal structures in Drosophila, Tribolium, and Locusta. Genes Dev 8, 2137-2150.

Knight, R.D., Mebus, K., Roehl, H.H., 2008. Mandibular arch muscle identity is regulated by a conserved molecular process during vertebrate development. J Exp Zool B Mol Dev Evol 310, 355-369.

Kolm, P.J., Sive, H.L., 1995. Efficient hormone-inducible protein function in Xenopus laevis. Dev Biol 171, 267-272.

Krauss, S., Concordet, J.-P., Ingham, P.W., 1993. A functionally conserved homologue of the *Drosophila* segment polarity gene *hh* is expressed in tissues with polarizing activity in zebrafish embryos. Cell 75, 1431-1444.

Kudoh, T., Tsang, M., Hukriede, N.A., Chen, X., Dedekian, M., Clarke, C.J., Kiang, A., Schultz, S., Epstein, J.A., Toyama, R., Dawid, I.B., 2001. A gene expression screen in zebrafish embryogenesis. Genome research 11, 1979-1987.

bioRxiv preprint doi: https://doi.org/10.1101/766501; this version posted September 12, 2019. The copyright holder for this preprint (which was not certified by peer review) is the author/funder, who has granted bioRxiv a license to display the preprint in perpetuity. It is made available under aCC-BY-NC-ND 4.0 International license.

894 Lacalli, T.C., 2002. The dorsal compartment locomotory control system in amphioxus
895 larvae. J Morphol 252, 227-237.
896 Lee, H.C., Tseng, W.A., Lo, F.Y., Liu, T.M., Tsai, H.J., 2009. FoxD5 mediates anterior-
897 posterior polarity through upstream modulator Fgf signaling during zebrafish
898 somitogenesis. Dev Biol 336, 232-245.
899 Lewis, K.E., Currie, P.D., Roy, S., Schauerte, H., Haffter, P., Ingham, P.W., 1999. Control
900 of muscle cell-type specification in the zebrafish embryo by Hedgehog signalling. Dev
901 Biol 216, 469-480.
902 Lolas, M., Valenzuela, P.D., Tjian, R., Liu, Z., 2014. Charting Brachyury-mediated
903 developmental pathways during early mouse embryogenesis. Proc Natl Acad Sci U S
904 A 111, 4478-4483.
905 Lu, F., Langenbacher, A., Chen, J.N., 2017. Tbx20 drives cardiac progenitor formation and
906 cardiomyocyte proliferation in zebrafish. Dev Biol 421, 139-148.
907 Maguire, R.J., Isaacs, H.V., Pownall, M.E., 2012. Early transcriptional targets of MyoD link
908 myogenesis and somitogenesis. Dev Biol 371, 256-268.
909 Manning, A.J., Kimelman, D., 2015. Tbx16 and Msgn1 are required to establish directional
910 cell migration of zebrafish mesodermal progenitors. Dev Biol.
911 Maroon, H., Walshe, J., Mahmood, R., Kiefer, P., Dickson, C., Mason, I., 2002. Fgf3 and
912 Fgf8 are required together for formation of the otic placode and vesicle. Development
913 129, 2099-2108.
914 Martin, B.L., Kimelman, D., 2008. Regulation of canonical Wnt signaling by Brachyury is
915 essential for posterior mesoderm formation. Dev Cell 15, 121-133.
916 McDermott, A., Gustafsson, M., Elsam, T., Hui, C.C., Emerson, C.P., Jr., Borycki, A.G.,
917 2005. Gli2 and Gli3 have redundant and context-dependent function in skeletal muscle
918 formation. Development 132, 345-357.
919 Melby, A.E., Warga, R.M., Kimmel, C.B., 1996. Specification of cell fates at the dorsal
920 margin of the zebrafish gastrula. Development 122, 2225-2237.
921 Molven, A., Wright, C.V., Bremiller, R., De Robertis, E.M., Kimmel, C.B., 1990. Expression
922 of a homeobox gene product in normal and mutant zebrafish embryos: evolution of the
923 tetrapod body plan. Development 109, 279-288.
924 Morrow, Z.T., Maxwell, A.M., Hoshijima, K., Talbot, J.C., Grunwald, D.J., Amacher, S.L.,
925 2017. tbx6l and tbx16 are redundantly required for posterior paraxial mesoderm
926 formation during zebrafish embryogenesis. Dev Dyn 246, 759-769.
927 Mueller, R.L., Huang, C., Ho, R.K., 2010. Spatio-temporal regulation of Wnt and retinoic
928 acid signaling by tbx16/spadetail during zebrafish mesoderm differentiation. BMC
929 Genomics 11, 492.
930 Münsterberg, A.E., Kitajewski, J., Bumcrot, D.A., McMahon, A.P., Lassar, A.B., 1995.
931 Combinatorial signalling by sonic hedgehog and Wnt family members induces
932 myogenic bHLH gene expression in the somite. Genes and Development 9, 2911-
933 2922.
934 Nelson, A.C., Cutty, S.J., Gasiunas, S.N., Deplae, I., Stemple, D.L., Wardle, F.C., 2017. In
935 Vivo Regulation of the Zebrafish Endoderm Progenitor Niche by T-Box Transcription
936 Factors. Cell reports 19, 2782-2795.
937 Nikaido, M., Kawakami, A., Sawada, A., Furutani-Seiki, M., Takeda, H., Araki, K., 2002.
938 Tbx24, encoding a T-box protein, is mutated in the zebrafish somite-segmentation
939 mutant fused somites. Nature genetics 31, 195-199.
940 Ochi, H., Hans, S., Westerfield, M., 2008. Smarcd3 regulates the timing of zebrafish
941 myogenesis onset. J Biol Chem 283, 3529-3536.
942 Odenthal, J., Haffter, P., Vogelsang, E., Brand, M., Van Eeden, F.J.M., Furutani-Seiki, M.,
943 Granato, M., Hammerschmidt, M., Heisenberg, C.P., Jiang, Y.J., Kane, D.A., Kelsh,

bioRxiv preprint doi: https://doi.org/10.1101/766501; this version posted September 12, 2019. The copyright holder for this preprint (which was not certified by peer review) is the author/funder, who has granted bioRxiv a license to display the preprint in perpetuity. It is made available under aCC-BY-NC-ND 4.0 International license.

944 R.N., Mullins, M.C., Warga, R.M., Allende, M.L., Weinberg, E.S., Nusslein-Volhard, C.,
945 1996. Mutations affecting the formation of the notochord in the zebrafish, Danio rerio.
946 Development 123, 103-115.
947 Osborn, D.P., Li, K., Hinits, Y., Hughes, S.M., 2011. Cdkn1c drives muscle differentiation
948 through a positive feedback loop with Myod. Dev Biol 350, 464-475.
949 Papaioannou, V.E., 2014. The T-box gene family: emerging roles in development, stem
950 cells and cancer. Development 141, 3819-3833.
951 Placzek, M., Briscoe, J., 2018. Sonic hedgehog in vertebrate neural tube development.
952 International Journal of Developmental Biology 62, 225-234.
953 Pradeepa, M.M., 2017. Causal role of histone acetylations in enhancer function.
954 Transcription 8, 40-47.
955 Pradeepa, M.M., Grimes, G.R., Kumar, Y., Olley, G., Taylor, G.C., Schneider, R.,
956 Bickmore, W.A., 2016. Histone H3 globular domain acetylation identifies a new class
957 of enhancers. Nature genetics 48, 681-686.
958 Reifers, F., Bohli, H., Walsh, E.C., Crossley, P.H., Stainier, D.Y., Brand, M., 1998. *Fgf8* is
959 mutated in zebrafish *acerebellar* (*ace*) mutants and is required for maintenance of
960 midbrain-hindbrain boundary development and somitogenesis. Development 125,
961 2381-2395.
962 Rentzsch, F., Bakkers, J., Kramer, C., Hammerschmidt, M., 2004. Fgf signaling induces
963 posterior neuroectoderm independently of Bmp signaling inhibition. Dev Dyn 231, 750-
964 757.
965 Rhinn, M., Lun, K., Luz, M., Werner, M., Brand, M., 2005. Positioning of the midbrain-
966 hindbrain boundary organizer through global posteriorization of the neuroectoderm
967 mediated by Wnt8 signaling. Development 132, 1261-1272.
968 Roelink, H., Augsburger, A., Heemskerk, J., Korzh, V., Norlin, S., Ruiz i Altaba, A.,
969 Tanabe, Y., Placzek, M., Edlund, T., Jessell, T.M., Dodd, J., 1994. Floor plate and
970 motor neuron induction by vhh-1, a vertebrate homolog of hedgehog expressed by the
971 notochord. Cell 76, 761-775.
972 Row, R.H., Maitre, J.L., Martin, B.L., Stockinger, P., Heisenberg, C.P., Kimelman, D.,
973 2011. Completion of the epithelial to mesenchymal transition in zebrafish mesoderm
974 requires Spadetail. Dev Biol 354, 102-110.
975 Rudnicki, M.A., Schnegelsberg, P.N., Stead, R.H., Braun, T., Arnold, H.H., Jaenisch, R.,
976 1993. MyoD or Myf-5 is required for the formation of skeletal muscle. Cell 75, 1351-
977 1359.
978 Ruvinsky, I., Silver, L.M., Ho, R.K., 1998. Characterization of the zebrafish tbx16 gene and
979 evolution of the vertebrate T-box family. Development genes and evolution 208, 94-99.
980 Satoh, N., Tagawa, K., Takahashi, H., 2012. How was the notochord born? Evolution &
981 Development 14, 56-75.
982 Schulte-Merker, S., Hammerschmidt, M., Beuchle, D., Cho, K.W., De Robertis, E.M.,
983 Nüsslein-Volhard, C., 1994a. Expression of zebrafish *goosecoid* and *no tail* gene
984 products in wild-type and mutant *no tail* embryos. Development 120, 843-852.
985 Schulte-Merker, S., van Eeden, F.J.M., Halpern, M.E., Kimmel, C.B., Nüsslein-Volhard, C.,
986 1994b. *no tail (ntl)* is the zebrafish homologue of the mouse *T (Brachyury)* gene.
987 Development 120, 1009-1015.
988 Showell, C., Binder, O., Conlon, F.L., 2004. T-box genes in early embryogenesis. Dev Dyn
989 229, 201-218.
990 Slack, J.M., Darlington, B.G., Heath, J.K., Godsave, S.F., 1987. Mesoderm induction in
991 early Xenopus embryos by heparin-binding growth factors. Nature 326, 197-200.

bioRxiv preprint doi: https://doi.org/10.1101/766501; this version posted September 12, 2019. The copyright holder for this preprint (which was not certified by peer review) is the author/funder, who has granted bioRxiv a license to display the preprint in perpetuity. It is made available under aCC-BY-NC-ND 4.0 International license.

992 Smith, J.C., Price, B.M., Green, J.B., Weigel, D., Herrmann, B.G., 1991. Expression of a
993 Xenopus homolog of Brachyury (T) is an immediate-early response to mesoderm
994 induction. Cell 67, 79-87.
995 Sun, X., Meyers, E.N., Lewandoski, M., Martin, G.R., 1999. Targeted disruption of Fgf8
996 causes failure of cell migration in the gastrulating mouse embryo. Genes Dev 13,
997 1834-1846.
998 Talbot, W.B., Trevarrow, B., Halpern, M.E., Melby, A.E., Farr, G., Postlethwait, T.J.,
999 Kimmel, C.B., Kimelman, D., 1995. A homeobox gene essential for zebrafish
1000 notochord development. Nature 378, 150-157.
1001 Taylor, M.V., Hughes, S.M., 2017. Mef2 and the skeletal muscle differentiation program.
1002 Semin Cell Dev Biol 72, 33-44.
1003 Tazumi, S., Yabe, S., Uchiyama, H., 2010. Paraxial T-box genes, Tbx6 and Tbx1, are
1004 required for cranial chondrogenesis and myogenesis. Dev Biol 346, 170-180.
1005 Thisse, B., Thisse, C., 2005. Functions and regulations of fibroblast growth factor signaling
1006 during embryonic development. Dev Biol 287, 390-402.
1007 Valasek, P., Theis, S., DeLaurier, A., Hinits, Y., Luke, G.N., Otto, A.M., Minchin, J., He, L.,
1008 Christ, B., Brooks, G., Sang, H., Evans, D.J., Logan, M., Huang, R., Patel, K., 2011.
1009 Cellular and molecular investigations into the development of the pectoral girdle. Dev
1010 Biol 357, 108-116.
1011 van Eeden, F.J., Granato, M., Schach, U., Brand, M., Furutani-Seiki, M., Haffter, P.,
1012 Hammerschmidt, M., Heisenberg, C.P., Jiang, Y.J., Kane, D.A., Kelsh, R.N., Mullins,
1013 M.C., Odenthal, J., Warga, R.M., Allende, M.L., Weinberg, E.S., Nüsslein-Volhard, C.,
1014 1996. Mutations affecting somite formation and patterning in the zebrafish, Danio rerio.
1015 Development 123, 153-164.
1016 van Eeden, F.J., Holley, S.A., Haffter, P., Nüsslein-Volhard, C., 1998. Zebrafish
1017 segmentation and pair-rule patterning. Dev Genet 23, 65-76.
1018 Warga, R.M., Mueller, R.L., Ho, R.K., Kane, D.A., 2013. Zebrafish Tbx16 regulates
1019 intermediate mesoderm cell fate by attenuating Fgf activity. Dev Biol 383, 75-89.
1020 Weinberg, E.S., Allende, M.L., Kelly, C.S., Abdelhamid, A., Murakami, T., Andermann, P.,
1021 Doerre, O.G., Grunwald, D.J., Riggleman, B., 1996. Developmental regulation of
1022 zebrafish MyoD in wild-type, no tail and spadetail embryos. Development 122, 271-
1023 280.
1024 Westerfield, M., 2000. The Zebrafish Book - A guide for the laboratory use of zebrafish
1025 (Danio rerio). University of Oregon Press.
1026 White, P.H., Farkas, D.R., McFadden, E.E., Chapman, D.L., 2003. Defective somite
1027 patterning in mouse embryos with reduced levels of Tbx6. Development 130, 1681-
1028 1690.
1029 Wilkinson, D.G., Peters, G., Dickson, C., McMahon, A.P., 1988. Expression of the FGF-
1030 related proto-oncogene int-2 during gastrulation and neurulation in the mouse. EMBO
1031 J 7, 691-695.
1032 Windner, S.E., Bird, N.C., Patterson, S.E., Doris, R.A., Devoto, S.H., 2012. Fss/Tbx6 is
1033 required for central dermomyotome cell fate in zebrafish. Biology open 1, 806-814.
1034 Windner, S.E., Doris, R.A., Ferguson, C.M., Nelson, A.C., Valentin, G., Tan, H., Oates,
1035 A.C., Wardle, F.C., Devoto, S.H., 2015. Tbx6, Mesp-b and Ripply1 regulate the onset
1036 of skeletal myogenesis in zebrafish. Development 142, 1159-1168.
1037 Woollard, A., Hodgkin, J., 2000. The caenorhabditis elegans fate-determining gene mab-9
1038 encodes a T-box protein required to pattern the posterior hindgut. Genes Dev 14, 596-
1039 603.

bioRxiv preprint doi: https://doi.org/10.1101/766501; this version posted September 12, 2019. The copyright holder for this preprint (which was not certified by peer review) is the author/funder, who has granted bioRxiv a license to display the preprint in perpetuity. It is made available under aCC-BY-NC-ND 4.0 International license.

Yamamoto, A., Amacher, S.L., Kim, S.H., Geissert, D., Kimmel, C.B., De Robertis, E.M., 1998. Zebrafish paraxial protocadherin is a downstream target of spadetail involved in morphogenesis of gastrula mesoderm. Development 125, 3389-3397.

Yamauchi, H., Miyakawa, N., Miyake, A., Itoh, N., 2009. Fgf4 is required for left-right patterning of visceral organs in zebrafish. Dev Biol 332, 177-185.

Yasuoka, Y., Shinzato, C., Satoh, N., 2016. The Mesoderm-Forming Gene brachyury Regulates Ectoderm-Endoderm Demarcation in the Coral Acropora digitifera. Current Biology 26, 2885-2892.

Yin, J., Lee, R., Ono, Y., Ingham, P.W., Saunders, T.E., 2018. Spatiotemporal Coordination of FGF and Shh Signaling Underlies the Specification of Myoblasts in the Zebrafish Embryo. Dev Cell 46, 735-750 e734.

Zeng, X.X., Wilm, T.P., Sepich, D.S., Solnica-Krezel, L., 2007. Apelin and its receptor control heart field formation during zebrafish gastrulation. Dev Cell 12, 391-402.

Zhang, X.M., Ramalho-Santos, M., McMahon, A.P., 2001. Smoothened mutants reveal redundant roles for Shh and Ihh signaling including regulation of L/R asymmetry by the mouse node. Cell 105, 781-792.

Fig. 1. Inhibition of Fgf signalling blocks initial induction of *myod* and *myf5* expression

In situ mRNA hybridization for *myod* and *myf5* in control untreated, cyclopamine-treated (cyA, 100 μM), SU5402-treated and double SU5402- and cyA-treated wild type or mutant embryos, shown in dorsal view, anterior to top. **A.** Adaxial (arrows) and paraxial *myod* and *myf5* mRNAs are lost upon SU5402-treatment (60 μM) from 30% to 80 or 90% epiboly (dashes indicate approximate position of germ ring) but are unaffected by cyA treatment. The anterior mesoderm marker *aplnrb* is normally down-regulated in paraxial presomitic cells expressing *myf5* (white dashes) and up-regulated in adaxial cells (arrow). Both changes were absent after SU5402-treatment. Schematics illustrate the location of equivalent cell types at two successive stages. mpcs = muscle precursor cells, CNH = chordoneural hinge (hatched), PSM = presomitic mesoderm (brackets). **B.** *Smo^{b641}* mutants retain pre-adaxial *myod* mRNA at 6ss even after cyA treatment, but lack pre-adaxial *myod* mRNA at 15ss. *Ptc1* mRNA downregulation shows that both *smo* mutation and cyA treatment (shown after longer colour reaction) fully block Hh signalling throughout the axis. Bars: 50 μm.

bioRxiv preprint doi: https://doi.org/10.1101/766501; this version posted September 12, 2019. The copyright holder for this preprint (which was not certified by peer review) is the author/funder, who has granted bioRxiv a license to display the preprint in perpetuity. It is made available under aCC-BY-NC-ND 4.0 International license.

Fig. 2. Successive Fgf and Hh signals drive trunk slow myogenesis

Immunodetection of slow MyHC in *shha* and *noto* mutants. **A.** Reduction in slow fibres in *shha* mutants is greater in tail than in trunk. Insets show individual fibres magnified. Upper graph shows mean ± SD of slow fibre number in the indicated somites from ten independent embryos of each genotype. Lower graph shows fraction of wild type fibres remaining in mutant. **B.** Trunk-specific residual slow muscle in *noto* mutant. **C.** 5-somite stage (5ss) embryos from a *noto*^{n1} heterozygote incross treated with cyA at 30% epiboly stage, showing loss of adaxial *myod* mRNA in anterior presomitic mesoderm (arrowheads), but retention in the most posterior pre-adaxial mesoderm (arrows) flanking the chordoneural hinge (white outline). **D.** SU5402 (50 µM) from tailbud stage ablates residual pre-adaxial *myod* and *myf5* mRNAs in cyA-treated 8ss embryos (arrows). Expression of paraxial *myod* in fast muscle precursors (asterisks) is not affected by cyA but is decreased by SU5402. Bars: 50 µm.

Fig. 3. Dorsally-expressed Fgfs drive paraxial myogenesis

In situ mRNA hybridization for *myod* and *myf5* (A,C) or *aplnrb* (D) mRNAs at 80% epiboly or *tbxta* (red) and *myod* (blue/brown) at tailbud stage (tb) (B). **A.** Reduction of *myod* and *myf5* mRNAs in *dual and triple fgf* MO-injected wild type embryos. Arrowheads indicate nascent adaxial cells. B**.** In contrast to 80% epiboly (compare Fig. S3C), at tailbud stage, cyclopamine (cyA) treatment ablates anterior adaxial *myod* mRNA, but leaves pre-adaxial expression intact (arrowheads). Injection of *fgf4+fgf8a* MOs ablate residual *myod* mRNA. **C.** Fgf4 or Fgf6a mRNA injection up-regulates *myod* and *myf5* mRNAs around the marginal zone. Note the widening of the unlabelled dorsal midline region (brackets). Insets show the same embryos viewed from vegetal pole. **D.** Fgf4 mRNA injection down-regulates *aplnrb* mRNA around the marginal zone (white dashes) but not anteriorly (brackets) in the dorsalized embryo. Bars: 100 µm.

Fig. 4 Redundant Fgf/Tbx and Hh signals required for MRF induction

In situ mRNA hybridization for *tbxta* and *tbx16* in control untreated and SU5402-treated from 30% embryos (A), for *myod, myf5, fgf8a*, *fgf*3 and *fgf4*, in control, *tbxta* MO- and *tbx16* MO-injected wild type (wt) embryos (B), and for *myod* and *myf5* in control, *tbxta* MO- and *tbx16* MO-injected wt embryos treated with or without 0.1 mM cyA (C). **A.** In 10 µM SU5402-treated wt embryos, *tbxta* and *tbx16* transcripts are decreased (arrows) at 80% epiboly, but almost normal at 6ss. Both transcripts are absent in 30 µM SU5402-treated

bioRxiv preprint doi: https://doi.org/10.1101/766501; this version posted September 12, 2019. The copyright holder for this preprint (which was not certified by peer review) is the author/funder, who has granted bioRxiv a license to display the preprint in perpetuity. It is made available under aCC-BY-NC-ND 4.0 International license.

embryos at 6ss. **B.** Adaxial *myod* expression (black arrowheads) is completely ablated in *tbxta* or *tbx16* morphants at 80% epiboly, and *myf5* expression is greatly decreased. *Fgf8a* mRNA is ablated in posterior notochord of *tbxta* morphants (blue arrowheads), but upregulated in *tbx16* morphants around the germ marginal zone at 80% and in posterior notochord at 6ss (yellow arrowheads). Expression of *fgf3* and *fgf4* is absent in posterior notochord of *tbxta* morphants, but enhanced in that location in *tbx16* morphants (green arrowheads). **C.** At 6ss, pre-adaxial *myod* expression (black arrowheads) is lost in *tbxta* morphant tailbud, and diminished in *tbx16* morphants. Injection of *tbx16* MO, but not *tbxta* MO, reduces adaxial *myf5* mRNA to the level in paraxial mesoderm (orange arrowheads), whereas *tbxta* MO but not *tbx16* MO up-regulates *myf5* mRNA in posterior tailbud (asterisks). *Tbx16* MO abolishes pre-adaxial *myf5* mRNA in cyA-treated embryos (white arrowheads). Adaxial *myf5* and *myod* transcripts recover in *tbxta* morphants, but are ablated by cyA-treatment (red arrowheads). CyA-treatment of *tbx16* morphants ablates adaxial *myod* expression throughout the axis (cyan arrowheads), leaving only residual paraxial *myod* and *myf5* expression (mauve arrowheads). Bars: 100 μm.

Fig. 5. Tbx16 is necessary and sufficient for MRF induction

In situ mRNA hybridization for the indicated mRNAs of control uninjected and *fgf4* (A,B) or *tbx16* (C,D) mRNA-injected embryos at 80% epiboly stage in *tbx16*$^{+/-}$ incross (A) and wild type (B-D). Dorsal views. Insets ventral views. **A.** *Myf5* and *myod* mRNAs flank the dorsal midline in siblings (sib), but are absent or greatly diminished in *tbx16*$^{-/-}$ mutants. *Fgf4* widened notochord (bars) and induced ectopic *myod* and *myf5* mRNA around the germ marginal zone of siblings, but did not rescue expression in *tbx16*$^{-/-}$ embryos. **B.** *Tbxta* mRNA reveals widened notochord (bars) in wild type embryos injected with *fgf4* mRNA. Both *tbxta* and *tbx16* mRNAs show clumping in the germ ring after overexpression of *fgf4*. **C,D.** *In situ* mRNA hybridization at 80% epiboly stage for *myf5* and *myod* mRNAs in wild type control or *tbx16* mRNA-injected embryos treated with SU5402 at 10 μM (C) or 60 μM (D). *Myf5* and *myod* mRNAs are ectopically induced in posterior mesoderm by Tbx16 expression, decreased by administration of 10 μM SU5402 in wild type, and rescued in SU5402-treated embryos by overexpression of *tbx16*. High dose SU5402 prevents MRF expression, even after *tbx16* mRNA injection. Bars: 100 μm.

bioRxiv preprint doi: https://doi.org/10.1101/766501; this version posted September 12, 2019. The copyright holder for this preprint (which was not certified by peer review) is the author/funder, who has granted bioRxiv a license to display the preprint in perpetuity. It is made available under aCC-BY-NC-ND 4.0 International license.

Fig. 6. *Myf5 is a direct transcriptional target of Tbx16*

A,B. Chromatin immunoprecipitation followed by sequencing (ChIP-seq) on wild-type (wt) embryos at 75-85% epiboly reveals endogenous Tbx16 and Tbxta binding events within 120 kb flanking the *myf5* transcriptional start site (TSS). RPM – ChIP-seq peak height in reads per million reads. H3K4me3 indicates TSSs. H3K4me1 indicates putative enhancers. H3K27ac indicates active enhancers. Known transcripts with exons (black) and introns (arrowheads) are indicated. Multiz Alignments & Conservation from UCSC Genome Browser (Haeussler et al., 2019) are shown beneath. Purple boxes indicate validated Tbx16 binding sites. Blue box indicates region expanded in panel B. Cyan boxes indicate other Tbx sites mentioned in text. **C**. ChIP-qPCR validation of Tbx16 peaks on *myf5* distal element (5DE) and proximal element 2 (5PE1). Error bars indicate standard error of the mean for biological triplicate experiments. **D.** Schematic showing how direct injection into wt embryos of mRNA encoding the Tbx16-Gulucocotorticoid Response fusion protein leads to target gene induction in the presence of protein synthesis inhibitor cycloheximide (CHD) induced by nuclear translocation triggered by dexamethasone (DEX). CHD caused ~5% delay in epiboly sowing it was active. **E.** Wild-type embryos injected with *tbx16-GR* mRNA treated with cycloheximide from germ ring stage and dexamethasone from shield stage. Note that embryos treated with cycloheximide alone exhibit wild type *myf5* expression at 75-80% epiboly, whereas embryos additionally treated with dexamethasone exhibit ectopic *myf5* expression with strong (white arrowheads, comparable to wt pre-adaxial level) and weak (black arrowheads, comparable to wt paraxial level) stain. Three separate CDH+DEX treated embryos are shown. Numbers indicate the fraction of embryos with the expression pattern(s) shown. Inset shows an unusual induction of *myf5* in anterior regions that was not observed with *myod*. **F.** Injection of *tbx16* mRNA (200 pg) into embryos from a *myf5*$^{hu2022/+}$ heterozygote incross led to ectopic up-regulation of *myod* mRNA in the dorsal germ ring (arrows) irrespective of genotype. Numbers indicate fraction of embryos showing ectopic mRNA/total analysed. Bars: 100 µm.

Fig. 7. Tbxta is essential for Fgf4-driven induction of *myod* but not *myf5*.

Embryos from a *tbxta*$^{+/-}$ incross injected with 150 pg *fgf4* mRNA or control. **A.** *Tbtxa*$^{-/-}$ mutants lack *myod* mRNA (arrows) but retain *myf5* mRNA in presomitic mesoderm (white dashes). *Fgf4* mRNA injection induced *myf5* and *myod* mRNAs throughout the posterior mesoderm in siblings (white dashes), but failed to induce *myod* mRNA in mutants. **B.** *Fgf4* suppressed *aplnrb* mRNA in posterior mesoderm above the germ ring (white dashes) in

bioRxiv preprint doi: https://doi.org/10.1101/766501; this version posted September 12, 2019. The copyright holder for this preprint (which was not certified by peer review) is the author/funder, who has granted bioRxiv a license to display the preprint in perpetuity. It is made available under aCC-BY-NC-ND 4.0 International license.

both *tbxta*$^{-/-}$ mutants and siblings. Individually genotyped embryos are shown in lateral view, dorsal to right (A,B). **C.** Scoring of *myod* mRNA accumulation in response to *Fgf4* mRNA injection into embryos from a *tbxta*$^{+/-}$ incross. Expanded: ventral expansion, generally all around germ ring as in panel A. Adaxial/faint: Either wild type pattern or faint version of it in small a small proportion of mutants, which was not significantly altered by Fgf4 mRNA. Left panel shows absolute number of embryos analysed from two experiments to emphasise lack of induction in mutants (raw data in Table S3). Right panel displays data as a percentage of the total to highlight reduced response in heterozygotes compared to wild type (X^2 test). **D.** Adaxial upregulation of *tbx16* mRNA is lost in *tbxta*$^{-/-}$ mutant (arrowheads). Fgf4 upregulates *tbx16* mRNA throughout ventral posterior mesoderm (arrows) and causes mesodermal cell aggregation (asterisks). *Tbxta*$^{-/-}$ mutants accumulate less *tbx16* mRNA than siblings and have less expression on the dorsal side (brackets). Bars: 100 μm.

Fig. 8. Tbx16 is essential for Fgf4-driven upregulation of *tbx16* and suppression of *tbxta*. Embryos from a *tbx16*$^{+/-}$ incross injected with 150 pg *fgf4* mRNA or control. **A,B.** By 24 hpf**,** Fgf4-injected embryos have disorganized heads and although lacking obvious trunk or tail, some contain twitching muscle (A). In situ mRNA hybridization for *col1a2* for dermomyotome/connective tissue and *myhz1* for skeletal muscle revealed muscle in *fgf4*-injected sibs, but not in *tbx16*$^{-/-}$ mutants (B). Boxes are magnified to show the alternating pattern of aggregated muscle and connective tissue in Fgf4-injected siblings, but the reduced *col1a2* and absent *myhz1* mRNA in Fgf4-injected mutants. Note the aggregation of posterior mesoderm cells into strands around the yolk. **C.** In situ mRNA hybridisation for *tbx16* mRNA in embryos from a *tbx16*$^{+/-}$ incross at around 90% epiboly. Nonsense mediate decay of the mutant transcript is apparent (arrow). Fgf4 RNA injection increases *tbx16* mRNA in paraxial mesoderm, widens dorsal axial notochord domain (asterisk) and causes aggregation of paraxial cells in siblings, but suppresses residual *tbx16* transcript in mutants. **D.** Immunodetection of Tbxt protein and *tbx16* mRNA in Fgf4-injected and control embryos from a *tbx16*$^{+/-}$ incross. A Fgf4-injected *tbx16*$^{-/-}$ mutant (bottom) reveals nuclear Tbxt protein in the entire posterior mesoderm. Residual *tbx16* mRNA in the prechordal region (arrows) but absence in posterior mesoderm demonstrates the genotype. **E.** Widespread up-regulation of *shha* mRNA reveals the notochord-like character of posterior mesoderm in Fgf4-injected *tbx16*$^{-/-}$ mutant. Bars: 100 μm.

Fig. 1

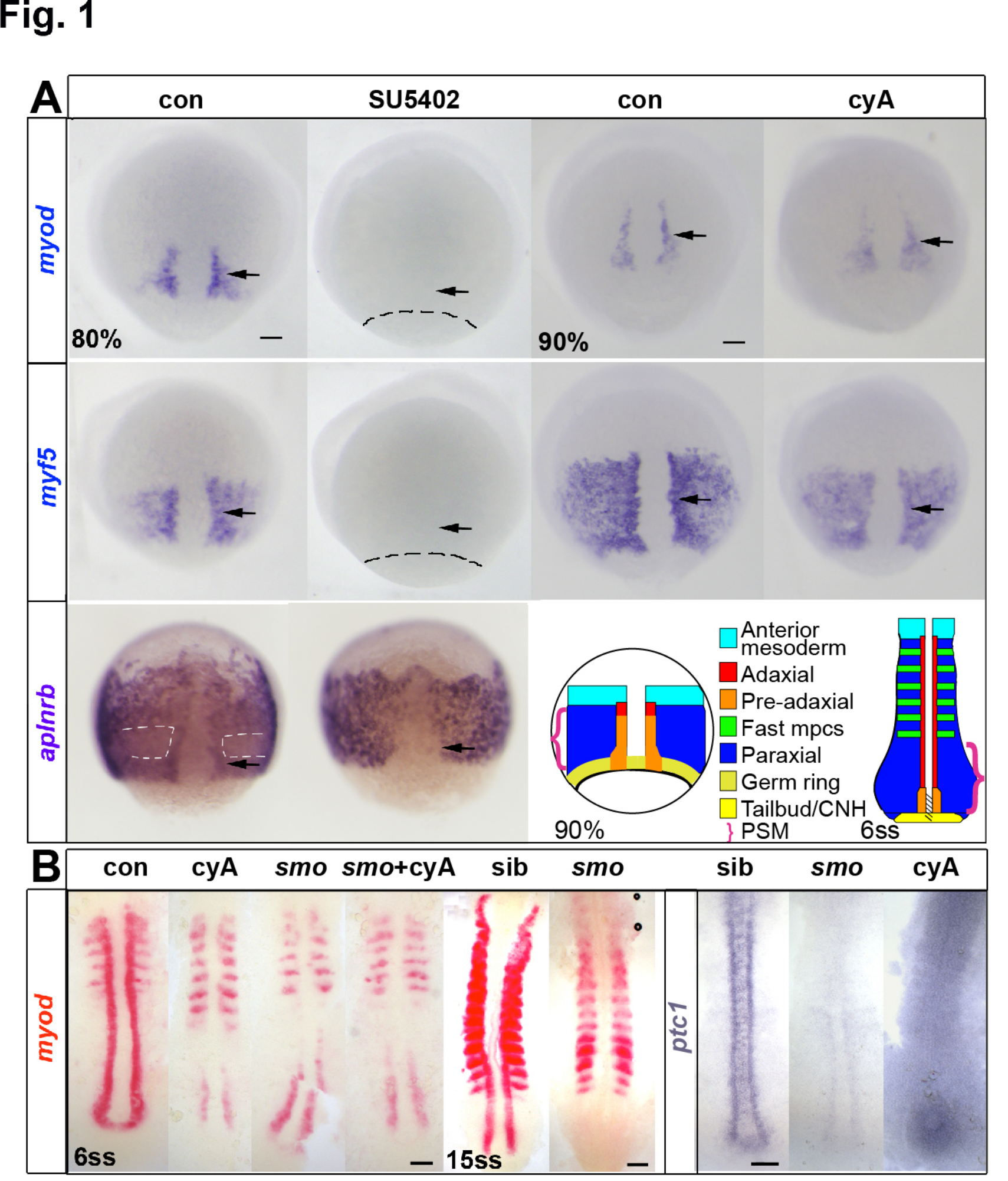
A
con
SU5402
con
cyA
myod
myf5
aplnrb
80%
90%
90%
Anterior mesoderm
Adaxial
Pre-adaxial
Fast mpcs
Paraxial
Germ ring
Tailbud/CNH
PSM
6ss
B
con
cyA
smo
smo+cyA
sib
smo
sib
smo
cyA
myod
ptc1
6ss
15ss

Fig. 2

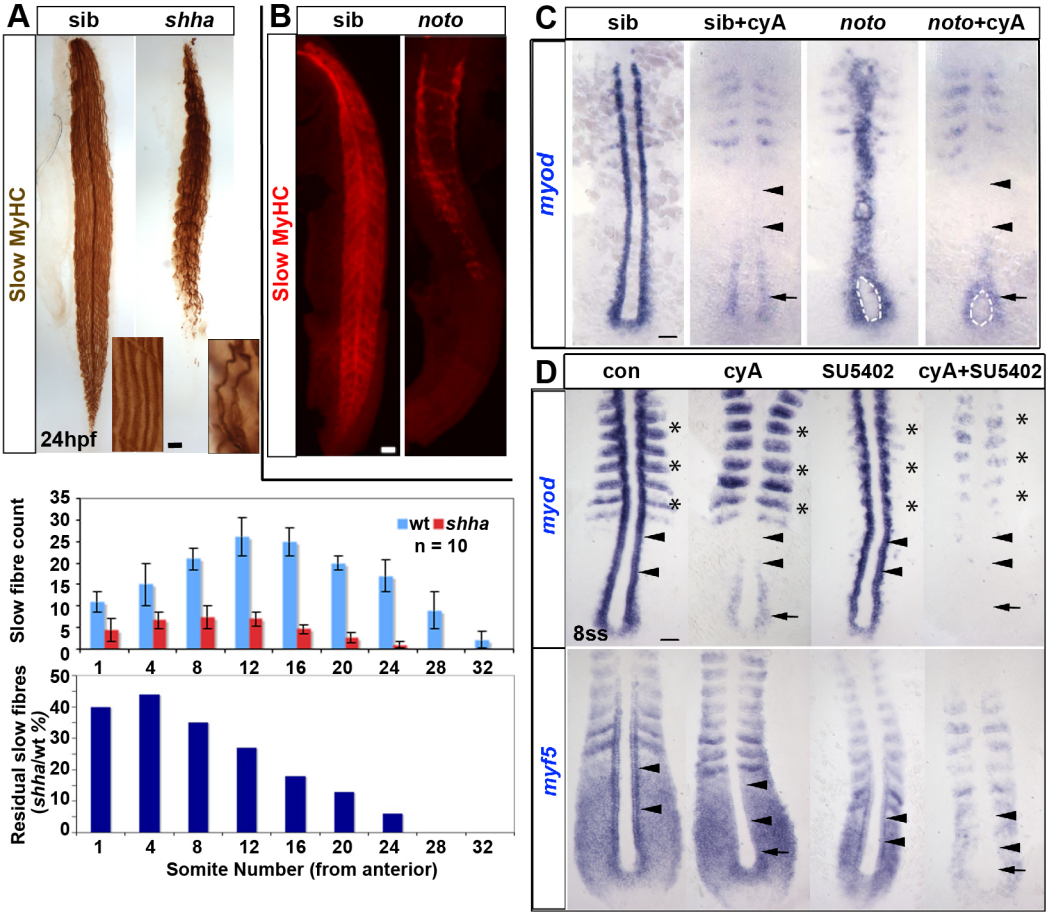
A
sib
shha
Slow MyHC
24hpf
B
sib
noto
Slow MyHC
C
sib
sib+cyA
noto
noto+cyA
myod
D
con
cyA
SU5402
cyA+SU5402
myod
8ss
myf5
Slow fibre count
wt
shha
n = 10
Residual slow fibres (shha/wt %)
Somite Number (from anterior)

Fig. 3

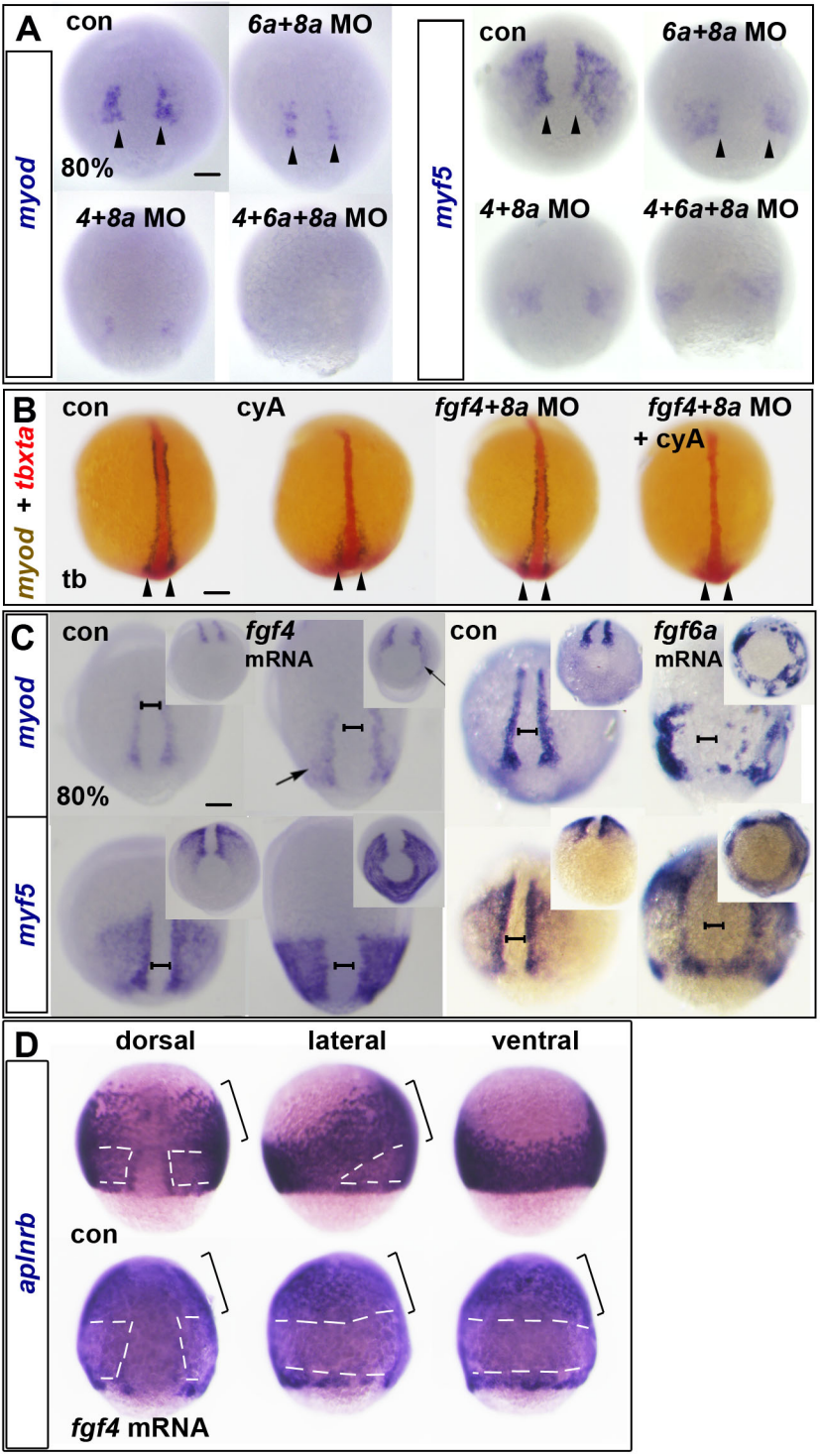
A
con
6a+8a MO
myod
80%
4+8a MO
4+6a+8a MO
myf5
con
6a+8a MO
4+8a MO
4+6a+8a MO
B
con
cyA
fgf4+8a MO
fgf4+8a MO
+ cyA
myod + tbxta
tb
C
con
fgf4
mRNA
con
fgf6a
mRNA
myod
80%
myf5
D
dorsal
lateral
ventral
aplnrb
con
fgf4 mRNA

Fig. 4

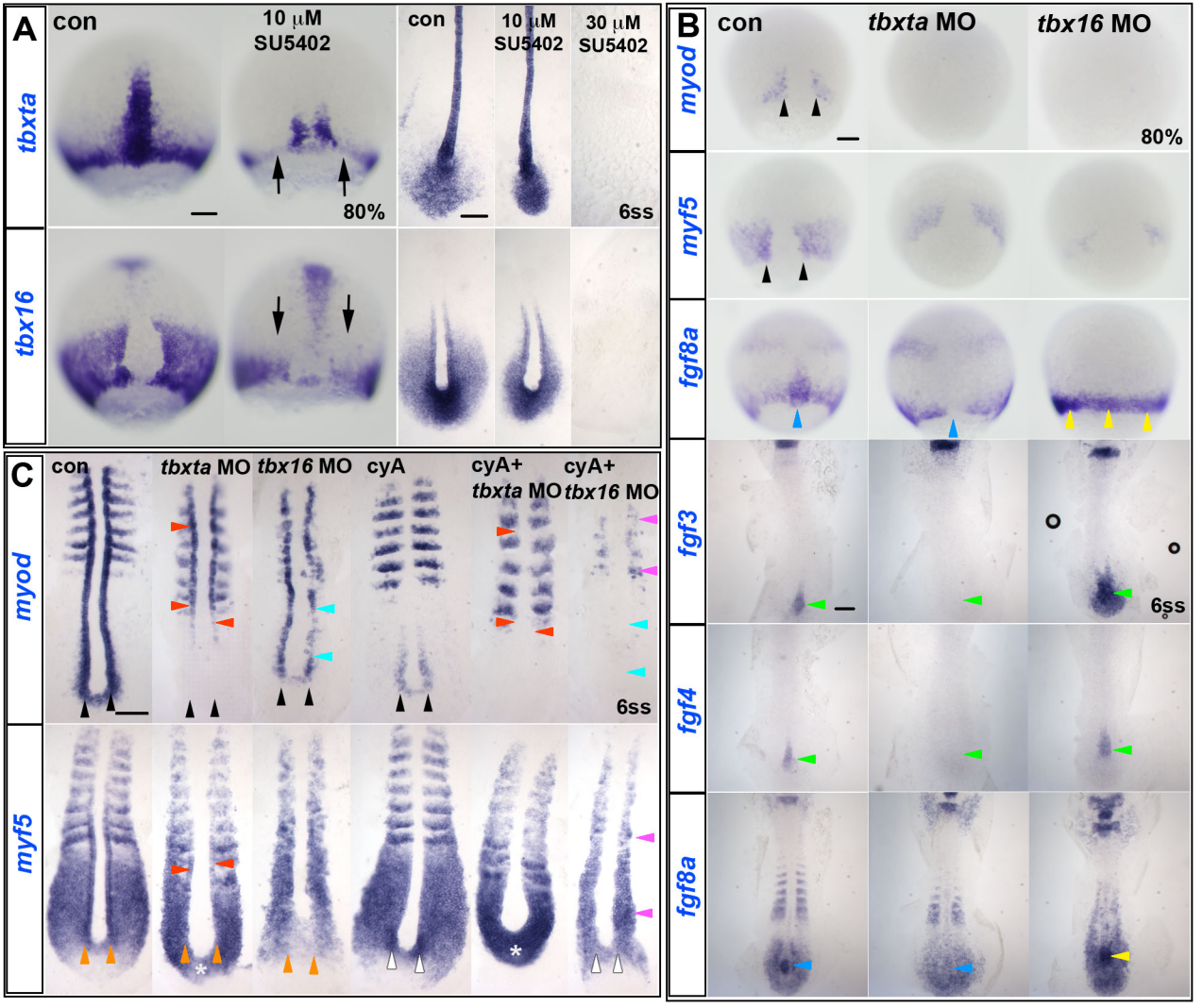
A
con
10 μM SU5402
con
10 μM SU5402
30 μM SU5402
tbxta
tbx16
80%
6ss
B
con
tbxta MO
tbx16 MO
myod
myf5
fgf8a
fgf3
fgf4
fgf8a
80%
6ss
C
con
tbxta MO
tbx16 MO
cyA
cyA+ tbxta MO
cyA+ tbx16 MO
myod
myf5
6ss

Fig. 5

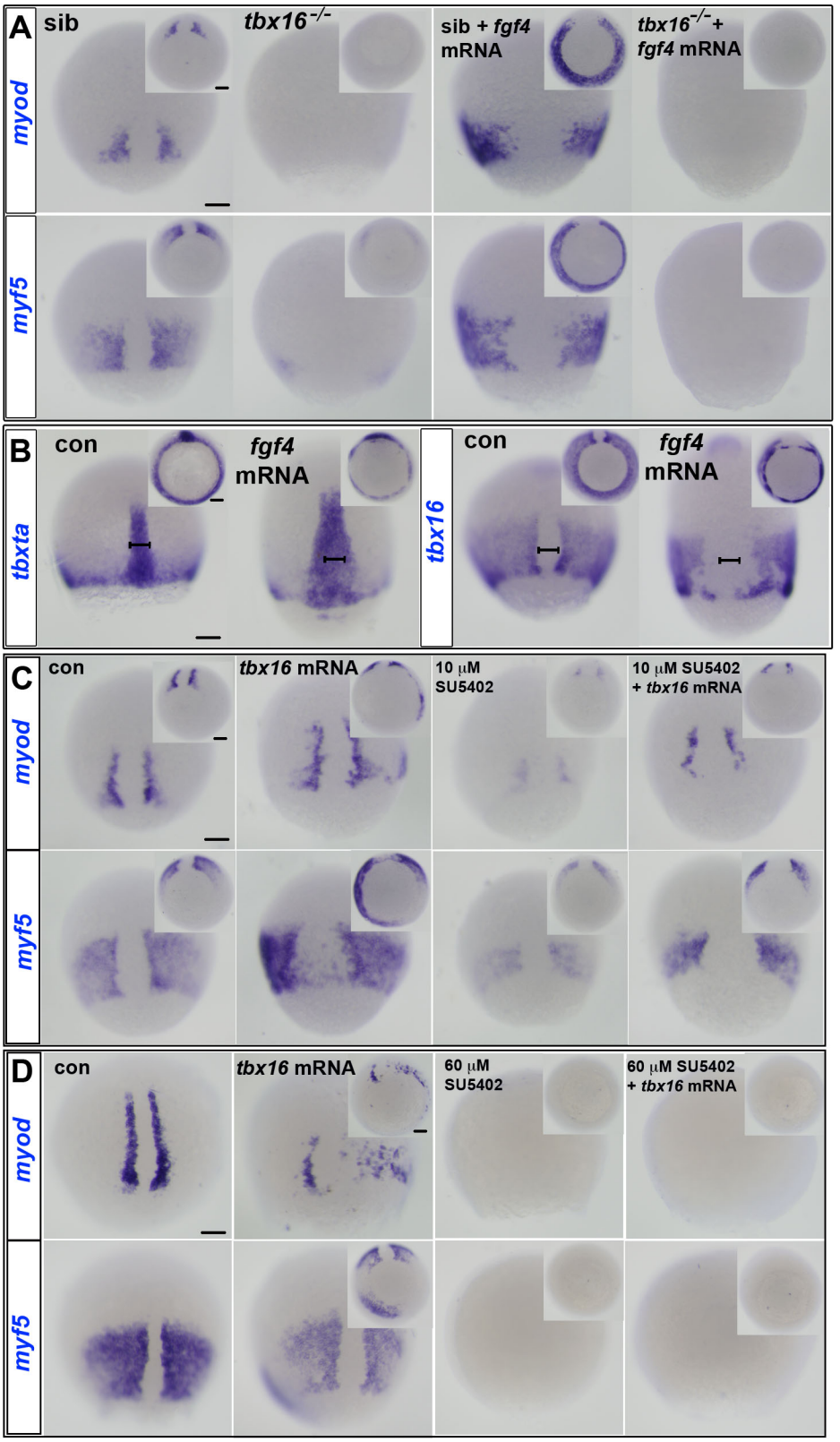
A
sib
tbx16-/-
sib + fgf4 mRNA
tbx16-/-+ fgf4 mRNA
myod
myf5
B
con
fgf4 mRNA
tbxta
tbx16
con
fgf4 mRNA
C
con
tbx16 mRNA
10 μM SU5402
10 μM SU5402 + tbx16 mRNA
myod
myf5
D
con
tbx16 mRNA
60 μM SU5402
60 μM SU5402 + tbx16 mRNA
myod
myf5

bioRxiv preprint doi: https://doi.org/10.1101/766501; this version posted September 12, 2019. The copyright holder for this preprint (which was not certified by peer review) is the author/funder, who has granted bioRxiv a license to display the preprint in perpetuity. It is made available under aCC-BY-NC-ND 4.0 International license.

Fig. 6

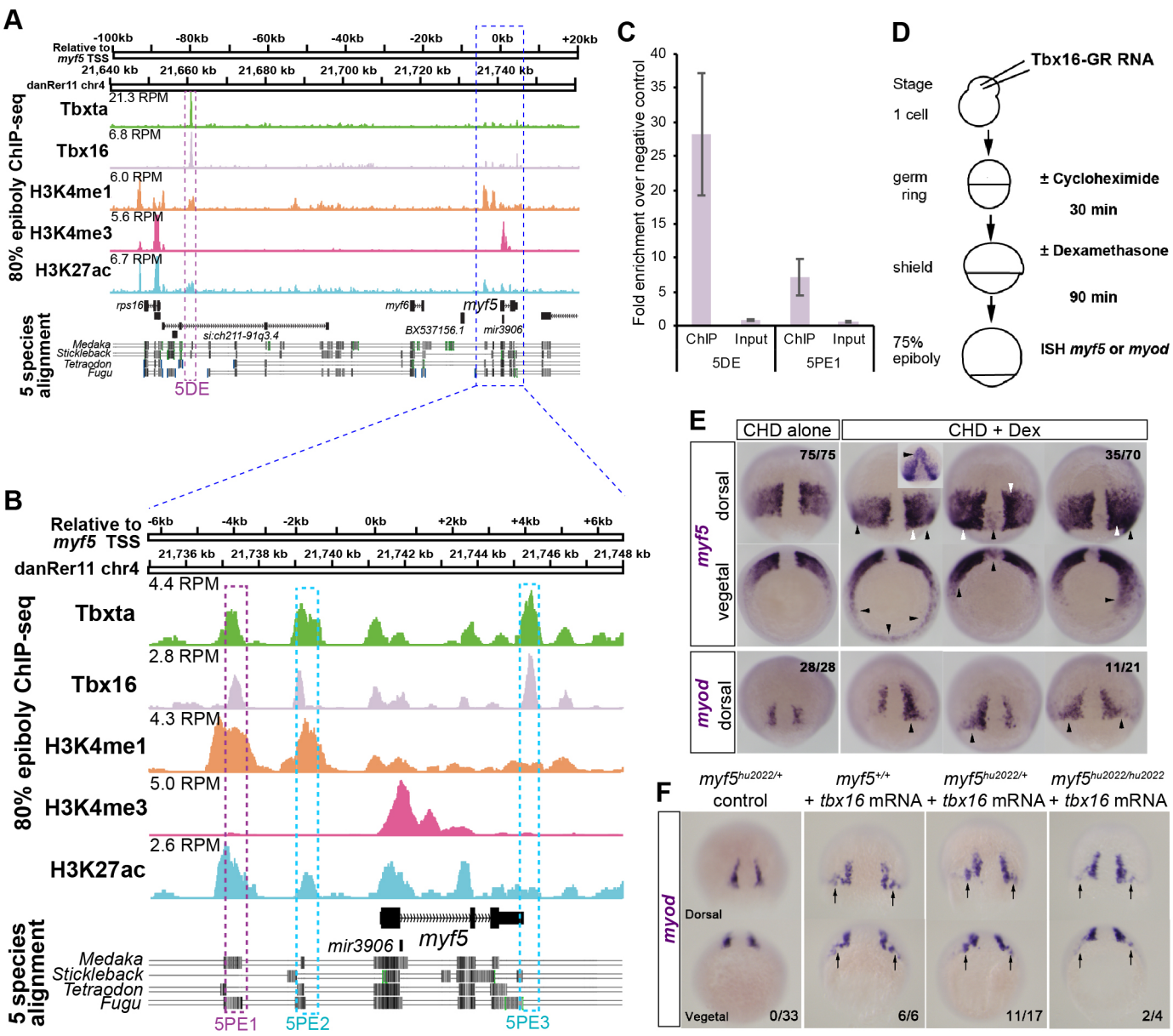

Fig. 7

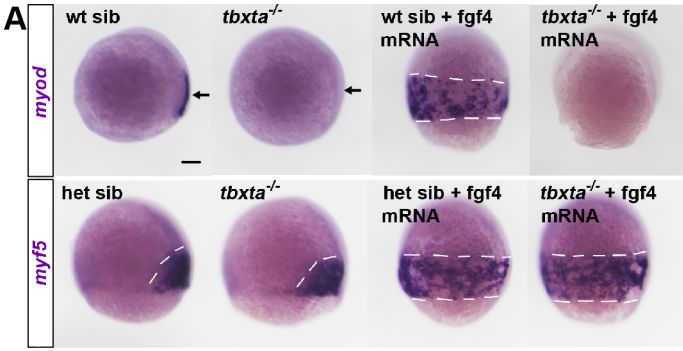
A
myod
wt sib
tbxta-/-
wt sib + fgf4 mRNA
tbxta-/- + fgf4 mRNA
myf5
het sib
tbxta-/-
het sib + fgf4 mRNA
tbxta-/- + fgf4 mRNA

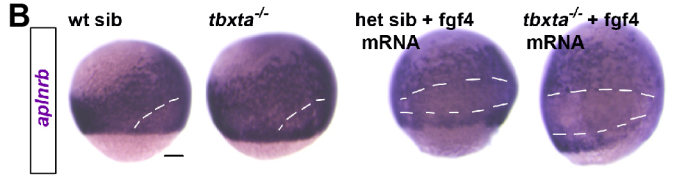
B
aplnrb
wt sib
tbxta-/-
het sib + fgf4 mRNA
tbxta-/- + fgf4 mRNA

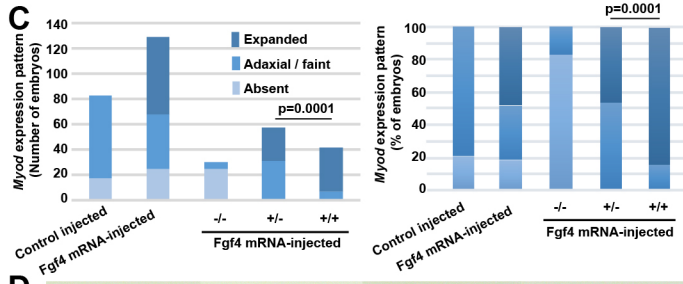
C
Myod expression pattern (Number of embryos)
Expanded
Adaxial / faint
Absent
p=0.0001
Control injected
Fgf4 mRNA-injected
-/-
+/-
+/+
Fgf4 mRNA-injected
Myod expression pattern (% of embryos)
p=0.0001

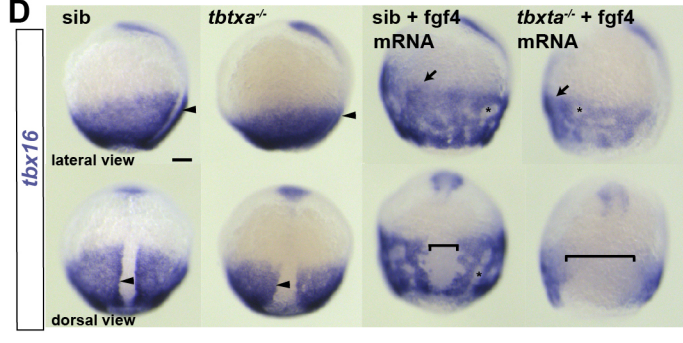
D
tbx16
sib
tbtxa-/-
sib + fgf4 mRNA
tbxta-/- + fgf4 mRNA
lateral view
dorsal view

available under aCC-BY-NC-ND 4.0 International license.

Fig. 8

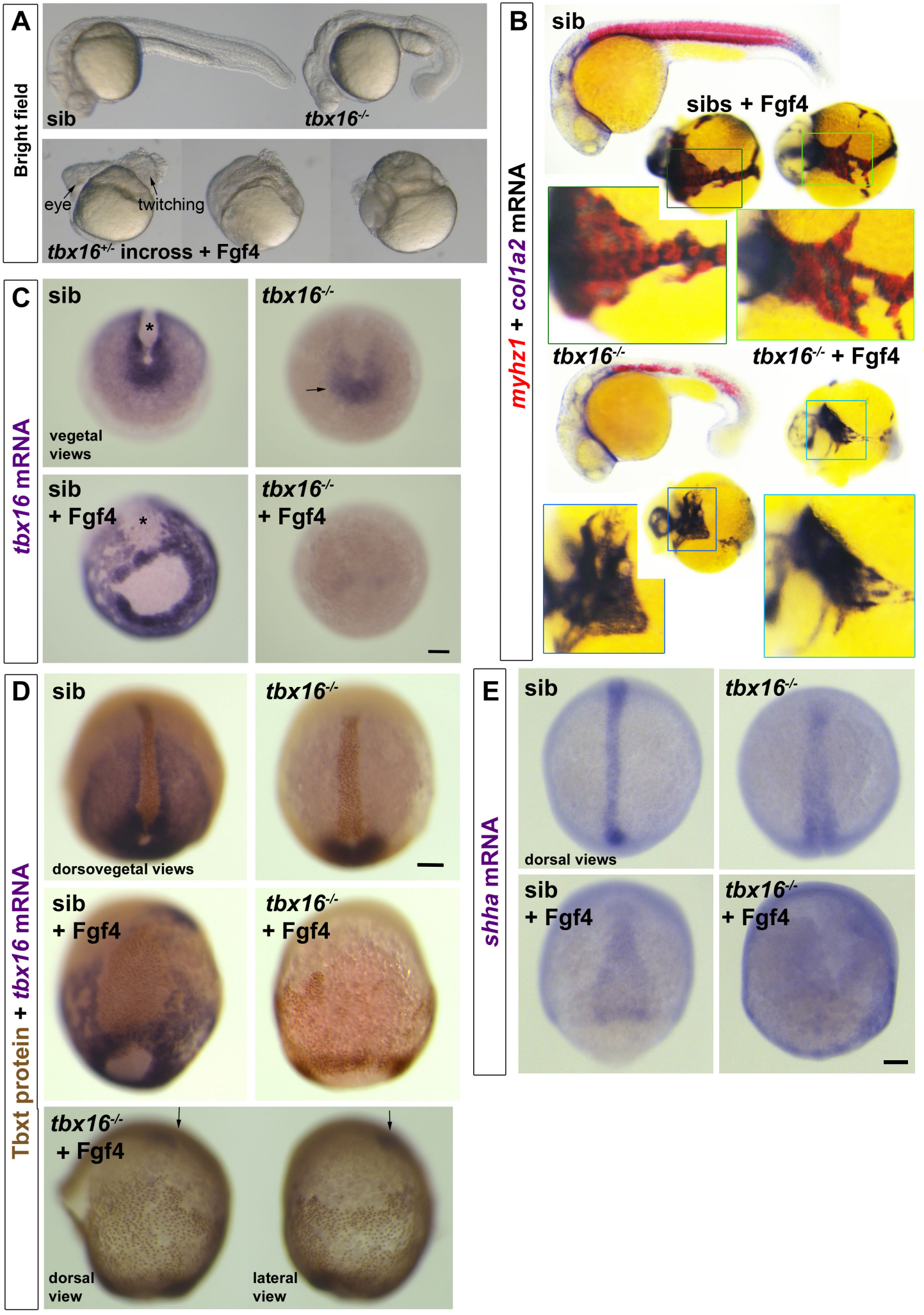

bioRxiv preprint doi: https://doi.org/10.1101/766501; this version posted September 12, 2019. The copyright holder for this preprint (which was not certified by peer review) is the author/funder, who has granted bioRxiv a license to display the preprint in perpetuity. It is made available under aCC-BY-NC-ND 4.0 International license.

1213 **Table S1 Quantitation of data in Figures**

Figure + panel	Assay	Treatment/genotype	Embryos with phenotype shown/Total (%)
1A	*myod* mRNA	con SU5402 con cyA	51/51 (100%) 40/40 (100%) 80/80 (100%) 60/60 (100%)
1A	*myf5* mRNA	con SU5402 con cyA	50/50 (100%) 36/36 (100%) 81/81 (100%) 68/68 (100%)
1A	*aplnrb* mRNA	con SU5402	30/30 (100%) 28/28 (100%)
1B	*myod* mRNA	cyA 6ss *smo* 6ss *smo* + cyA 6ss *smo* 15ss	83/83 (100%) 13/46 (28%) 14/54 (26%) 26/99 (26%)
1B	*ptc1* mRNA	*smo* 6ss cyA	11/67 (16%) 31/31 (100%)
2A	Slow MyHC	*shha* 24hpf	23/80 (29%)
2B	Slow MyHC	*noto* 24hpf	25/88 (28%)
2C	*myod* mRNA	sib *noto* sib + cyA *noto* + cyA	47/62 (76%) 15/62 (24%) 39/56 (70%) 17/56 (30%)
2D	*myod* mRNA	con cyA SU5402 SU5402 + cyA	67/67 (100%) 47/47 (100%) 116/116 (100%) 62/63 (98%)
2D	*myf5* mRNA	con cyA SU5402 SU5402+cyA	20/20 (100%) 15/15 (100%) 5/5 (100%) 13/13 (100%)
3A	*myod* mRNA	con *fgf6a* MO + *fgf8a* MO *fgf4* MO + *fgf8a* MO *fgf4* MO + *fgf6a* MO + *fgf8a* MO	35/40 (88%) + 8/19 (42%) 38/46 (83%) + 22/26 (85%) 25/36 (69%) 13/15 (87%)
3A	*myf5* mRNA	con *fgf6a* MO + *fgf8a* MO *fgf4* MO + *fgf8a* MO *fgf4* MO + *fgf6a* MO + *fgf8a* MO	38/40 (95%) + 20/20 (100%) 46/50 (97%) + 32/33 (91%) 11/38 (29%) 17/25 (68%)
3B	*myod* mRNA	con cyA f*gf4* MO + *fgf8a* MO f*gf4* MO + *fgf8a* MO + cyA	3/3 (100%) 5/5 (100%) 5/5 (100%) 4/5 (80%)
3C	*myod* mRNA	con (fgf4) +_*fgf4* mRNA con (fgf6a)	129/129 (100%) 131/136 (96%) 20/20 (100%)

bioRxiv preprint doi: https://doi.org/10.1101/766501; this version posted September 12, 2019. The copyright holder for this preprint (which was not certified by peer review) is the author/funder, who has granted bioRxiv a license to display the preprint in perpetuity. It is made available under aCC-BY-NC-ND 4.0 International license.

		+ *fgf6a* mRNA	20/20 (100%)
3C	*myf5* mRNA	con (fgf4)	30/30 (100%)
		+_*fgf4* mRNA	34/40 (85%)
		con (fgf6a)	20/20 (100%)
		+ *fgf6a* mRNA	18/18 (100%)
3D	*aplnrb* mRNA	con	32/32 (100%)
		+ *fgf4* mRNA	12/18 (67%)
4A	*tbxta* mRNA	con 80%	21/21 (100%)
		low SU5402 80%	14/14 (100%)
		con 6ss	52/52 (100%)
		low SU5402 6ss	44/50 (88%)
		high SU5402 6ss	32/32 (100%)
4A	*tbx16* mRNA	con 80%	21/21 (100%)
		low SU5402 80%	15/15 (100%)
		con 6ss	40/40 (100%)
		low SU5402 6ss	41/41 (100%)
		high SU5402 6ss	74/74 (100%)
4B	*myod* mRNA	con	28/28 (100%)
		tbxta MO	20/21 (95%)
		tbx16 MO	20/22 (91%)
4B	*myf5* mRNA	con	30/30 (100%)
		tbxta MO	12/19 (63%)
		tbx16 MO	19/20 (95%)
4B	*fgf8a* mRNA	con	30/30 (100%)
		tbxta MO	19/20 (95%)
		tbx16 MO	18/20 (90%)
4B	*fgf3* mRNA	con	25/25 (100%)
		tbxta MO	17/17 (100%)
		tbx16 MO	11/14 (79%)
4B	*fgf4* mRNA	con	28/28 (100%)
		tbxta MO	19/19 (100%)
		tbx16 MO	12/14 (86%)
4B	*fgf8a* mRNA	con	30/30 (100%)
		tbxta MO	14/16 (88%)
		tbx16 MO	10/12 (83%)
4C	*myod* mRNA	con	31/31 (100%)
		tbxta MO	21/22 (95%)
		tbx16 MO	24/24 (100%)
		cyA	30/30 (100%)
		cyA + tbxta MO	23/23 (100%)
		cyA + tbx16 MO	22/22 (100%)
4C	*myf5* mRNA	con	40/40 (100%)
		tbxta MO	24/26 (92%)
		tbx16 MO	25/25 (100%)
		cyA	38/38 (100%)
		cyA + tbxta MO	19/20 (95%)
		cyA + tbx16 MO	24/24 (100%)
5A	*myod* mRNA	sib	82/122 (67%)
		tbx16-/-	40/122 (33%)
		sib + fgf4 mRNA	95/128 (78%)
		tbx16-/- + fgf4 mRNA	33/128 (26%)
5A	*myf5* mRNA	sib	95/120 (79%)

bioRxiv preprint doi: https://doi.org/10.1101/766501; this version posted September 12, 2019. The copyright holder for this preprint (which was not certified by peer review) is the author/funder, who has granted bioRxiv a license to display the preprint in perpetuity. It is made available under aCC-BY-NC-ND 4.0 International license.

		tbx16-/- sib + fgf4 mRNA *tbx16-/-* + fgf4 mRNA	25/120 (21%) 98/126 (78%) 28/126 (22%)
5B	*tbxta* mRNA	con fgf4 mRNA	30/30 (100%) 20/21 (95%)
5B	*tbx16* mRNA	con fgf4 mRNA	29/29 (100%) 61/61 (100%)
5C	*myod* mRNA	con +tbx16 mRNA con + 10 μM SU5402 +tbx16 mRNA + 10 μM SU5402	31/31 (100%) 7/42 (17%) 32/32 (100%) 7/35 (20%)
5C	*myf5* mRNA	con +tbx16 mRNA con + 10 μM SU5402 +tbx16 mRNA + 10 μM SU5402	24/24 (100%) 14/42 (33%) 29/29 (100%) 4/35 (11%)
5D	*myf5* mRNA	con +tbx16 mRNA con + 60 μM SU5402 +tbx16 mRNA + 60 μM SU5402	18/18 (100%) 2/23 (9%), 21/23 (91%) faint 8/8 (100%) 23/23 (100%)
5D	*myod* mRNA	con +tbx16 mRNA con + 60 μM SU5402 +tbx16 mRNA + 60 μM SU5402	15/15/ (100%) 2/24 (8%), 7/24 (29%) disrupted 15/15 (100%) 32/32 (100%)
6E	*myf5* mRNA	CHD alone CHD + DEX	75/75 (100%) 35/70 (50%)
6E	*myod* mRNA	CHD alone CHD + DEX	28/28 (100%) 11/21 (52%)
6F	*myod* mRNA	Control *myf5* het incross *myf5*+/+ + tbx16 mRNA *myf5*+/- + tbx16 mRNA *myf5*-/- + tbx16 mRNA	33/33 (100%) 6/6 (100%) 11/17 (65%) 2/4 (50%)
7A	*myod* mRNA	sib *tbxta-/-* sib + *fgf4* mRNA *tbxta-/-* + *fgf4* mRNA	100/132 (76%) 32/132 (24%) 16/27 (59%) (for genotyping see 8/27 (29%) Table S4)
7A	*myf5* mRNA	sib *tbxta-/-* sib + *fgf4* mRNA *tbxta-/-* + *fgf4* mRNA	108/138 (78%) 30/138 (22%) 50/74 (68%) 24/74 (32%)
7B	*aplnrb* mRNA	sib *tbxta-/-* sib + *fgf4* mRNA *tbxta-/-* + *fgf4* mRNA	144/195 (74%) 51/195 (26%) 12/18 (67%) 6/18 (33%)
7D	*tbx16* mRNA	sib *tbxta-/-* sib + *fgf4* mRNA *tbxta-/-* + *fgf4* mRNA	48/66 (73%) 18/66 (27%) 70/93 (75%) 23/93 (25%)

bioRxiv preprint doi: https://doi.org/10.1101/766501; this version posted September 12, 2019. The copyright holder for this preprint (which was not certified by peer review) is the author/funder, who has granted bioRxiv a license to display the preprint in perpetuity. It is made available under aCC-BY-NC-ND 4.0 International license.

8A	Bright field	sib *tbx16-/-* + *fgf4* mRNA	28/41 (68%) 13/41 (32%) 48
8B	*myhz1* mRNA	sib *tbx16-/-* sib + *fgf4* mRNA *tbx16-/-* + *fgf4* mRNA	27/40 (68%) 13/40 (32%) 38/48 (79%) 10/48 (21%)
8C,D	*tbx16* mRNA+ Tbxta protein	sib *tbx16-/-* sib + *fgf4* mRNA *tbx16-/-* + *fgf4* mRNA	33/47 (70%) 14/47 (30%) 40/57 (70%) 17/57 (30%)
8E		sib *tbxt16-/-* sib + *fgf4* mRNA *tbx16-/-* + *fgf4* mRNA	19/28 (68%) 9/28 (32%) 19/31 (61%) 12/31 (39%)
S1	*aplnrb* mRNA	50%-10ss	approx. 25 embryos/stage
S2A	Slow MyHC	*smo* sib	27/40 (67.5%)
S2B	Slow MyHC	*smo* sib + *myod* mRNA	28/35 (80%)
S2C	Slow MyHC	*smo*$^{-/-}$	13/40 (32.5%)
S2D	Slow MyHC	*smo*$^{-/-}$ + *myod* mRNA	7/35 (20%)
S2E	Slow MyHC	con	100/100 (100%)
S2F	Slow MyHC	cyA	73/73 (100%)
S2G	Slow MyHC	cyA + *myod* mRNA	20/32 (63%)
S2H	Slow MyHC + Prox1 + GFP	cyA + *myog* mRNA	26/46 (57%)
S2I	Slow MyHC + Prox1	24hpf	50/50 (100%)
S2J	Slow MyHC + Prox1	24hpf	26/43 (60%)
S3B	*myod* mRNA	con + *fgf3* MO + *fgf4* MO + *fgf6a* MO *fgf8a-/-*	39/47 58/65 46/70 52/69
S3B	*myf5* mRNA	con + *fgf3* MO + *fgf4* MO + *fgf6a* MO *fgf8a-/-*	51/51 (100%) 21/58 (36%) 19/58 (33%) 44/69 (64%)
S3C	*myf5* mRNA	sib + con MO *fgf8a-/-* + con MO sib + triple Fgf MO *fgf8a-/-* + triple Fgf MO	13/17 (76%) (2/2 genotyped sib) 4/17 (24%) (3/4 genotyped -/-) 19/31 (77%) (2/2 genotyped sib) 7/31(23%) (3/3 genotyped -/-)
S3D	*myod mRNA*	con + *fgf4* MO + *fgf6a* MO + *fgf4* MO + *fgf6a* MO	4/4 3/3 2/2 3/3

bioRxiv preprint doi: https://doi.org/10.1101/766501; this version posted September 12, 2019. The copyright holder for this preprint (which was not certified by peer review) is the author/funder, who has granted bioRxiv a license to display the preprint in perpetuity. It is made available under aCC-BY-NC-ND 4.0 International license.

1217 **Table S2 Sequences of morpholinos and primers**

Morpholino			
Gene	**Sequence** (start codon underlined)	**Quantity (ng)**	**Reference**
fgf3	5'-CATTGTGGCATGGCGGGATGTCGGC-3'	7.5	(Maroon et al., 2002)
fgf4	5'-GCAAGAGGGCTGAC*T*GGACACTCAT-3'	2-6	
fgf6a	5'-TGAGGAACCTTTGCGCAGTGGCCAT-3'	2-6	
fgf8a	5'-GAGTCTCATGTTTATAGCCTCAGTA -3'	2	(Furthauer et al., 2001)
tbx16	5'-GCTTGAGGTCTCTGATAGCCTGCAT-3'	0.5	(Bisgrove et al., 2005)
tbxta	5'-GACTTGAGGCAG*G*CATATTTCCGAT -3' 5'-GCTGGTCGGGACTTGAGGCAGACAT-3'	0.25 2	(Bisgrove et al., 2005; Feldman and Stemple, 2001)
control	5'-CCTCCTACCTCAGTTACAATTTATA -3'	3-6	Gene Tools standard

Primers (start and stop codons underlined)			
Gene	**Forward**	**Reverse**	**Reference**
fgf4	5'-GAGCTCGAGCTCATGAGTGTCC AGTCGGCCCTCTTG-3'	5'-GTCGACGTCGACTCAAATTCTAGGCA AG-3'	
5DE_ChIP-qPCR	5'-TTCCTCACCGTACCTTTTGC-3'	5'-CATTTCCCCCACAATACACC-3'	
5PE1_ChIP-qPCR	5'-GTGCAATTTTGGCTCAGCTT-3'	5'-AGATCGGGGAACTTCGCTAT-3'	
Negative region (*rhod*)	5'-GACTCCACACAATCTGCAACAT-3'	5'-ACCACCTACGCTAAAGAAACCA-3'	Morley et al., 2009

1218

1219

Table S3 Location and histone modifications of Tbx16 and Tbxta ChIP-seq peaks on *myf5* and *myod* loci

Tbx16 ChIP-seq

***myf5* locus**

		Zv9/danRer7							GRCz11/danRer11			
Putative enhancer ID	**chr**	**start**	**stop**	**Tbx16 ChIP1 *P* value**	**Tbx16 ChIP2 *P* value**	**H3K4me1**	**H3K4me3**	**H3K27ac**	**start**	**stop**	**size**	**Distance from TSS to peak centre**
5DE	chr4	20596134	20597306	2.3659E-91	3.7325E-52	Yes	No	Yes	21660444	21661616	1173	-80198.5
5PE1	chr4	20672749	20673195	5.4702E-11	6.93426E-08	Yes	No	Yes	21737059	21737505	447	-3945.5
5PE3	chr4	20680778	20681312	1.6943E-08	1.96789E-06	No	No	No	21745088	21745622	535	+4126.5

***myod* locus**

Putative enhancer ID	**chr**	**start**	**stop**	**Tbx16 ChIP1 *P* value**	**Tbx16 ChIP2 *P* value**	**H3K4me1**	**H3K4me3**	**H3K27ac**	**start**	**stop**	**size**	**Distance from TSS to peak centre**
D3'E1	chr25	32256140	32256596	8.7498E-14	2.1727E-06	No	No	No	31412869	31413325	457	+10,396
DDE1	chr25	32297466	32298512	3.9264E-30	3.9355E-09	Yes	No	No	31454195	31455241	1047	-31224.5
DDE2	chr25	32307295	32307540	1.4555E-05	5.22396E-05	No	No	No	31464024	31464269	246	-40653

Tbxta ChIP-seq

***myf5* locus**

		Zv9/danRer7							GRCz11/danRer11			
Putative enhancer ID	**chr**	**start**	**stop**	**Tbxta ChIP1 *P* value**	**Tbxta ChIP2 *P* value**	**H3K4me1**	**H3K4me3**	**H3K27ac**	**start**	**stop**	**size**	**Distance from TSS to peak centre**
5DE	chr4	20595996	20597295	N.S.	2.8774E-90	Yes	No	Yes	21660306	21661605	1300	-80273
5PE2	chr4	20674923	20675240	4.4668E-06	1.1298E-13	Yes	No	No	21739233	21739550	318	-1837

***myod* locus**

Putative enhancer ID	**chr**	**start**	**stop**	**Tbxta ChIP1 *P* value**	**Tbxta ChIP2 *P* value**	**H3K4me1**	**H3K4me3**	**H3K27ac**	**start**	**stop**	**size**	**Distance from TSS to peak centre**
DDE1	chr25	32297085	32298653	N.S.	2.26464E-12	Yes	No	No	31453814	31455382	1569	-31104.5
DDE3	chr25	32312015	32312366	1.0864E-07	1.14551E-37	Yes	No	Yes	31468744	31469095	352	-45426

Peaks with significant H3K4me1 and H3K27ac

N.S. = not significant

bioRxiv preprint doi: https://doi.org/10.1101/766501; this version posted September 12, 2019. The copyright holder for this preprint (which was not certified by peer review) is the author/funder, who has granted bioRxiv a license to display the preprint in perpetuity. It is made available under aCC-BY-NC-ND 4.0 International license.

Table S4. Tbxta dosage controls response of *myod* to Fgf.

Fgf4 mRNA (pg)	Genotype	Number genotyped [%]¶	*Myod* mRNA expression pattern in genotyped embryos (%)		
			Absent	Adaxial only	Expanded ventrally
0	-/-	4*	4 (100%)§	0 (0%)	0 (0%)
	+/-	3*	0 (0%)	3 (100%)	0 (0%)
	+/+	2*	0 (0%)	2 (100%)	0 (0%)
	Total	9	8 ((15%))∞	45 ((85%))	0 ((0%))
100	-/-	8 [30%]	7 (88%)	1 (12%)	0 (0%)
	+/-	14 [52%]	0 (0%)	11 (79%)	3 (21%)
	+/+	5 [19%]	0 (0%)	0 (0%)	5 (100%)
	Total	27	7 (26%)	12 (44%)	8 (30%)
0	-/-	5*	5 (100%)	0 (0%)	0 (0%)
	+/-	2*	0 (0%)	2 (100%)	0 (0%)
	+/+	3*	0 (0%)	3 (100%)	0 (0%)
	Total	10	9 ((30%))	21 ((70%))	0 ((0%))
100	-/-	1 [6%]	1 (100%)	0 (0%)	0 (0%)
	+/-	8 [50%]	0 (0%)	3 (37%)	5 (63%)
	+/+	7 [44%]	0 (0%)	1 (14%)	6 (86%)
	Total	16	1 (6%)	4 (25%)	11 (69%)
150	-/-	6 [25%]	5 (100%)	1 (17%)	0 (0%)
	+/-	9 [38%]	0 (0%)	6 (67%)	3 (33%)
	+/+	9 [38%]	0 (0%)	2 (22%)	7 (78%)
	Total	24	5 (21%)	9 (38%)	10 (42%)
225	-/-	15 [24%]	12 (80%)	3 (20%)	0 (0%)
	+/-	26 [42%]	0 (0%)	11 (42%)	15 (58%)
	+/+	21 [34%]	0 (0%)	4 (19%)	17 (81%)
	Total	62	12 (19%)	18 (29%)	32 (52%)
Summary					
0	-/-	9*	9 (100%)	0 (0%)	0 (0%)
	+/-	5*	0 (0%)	5 (100%)	0 (0%)
	+/+	5*	0 (0%)	5 (100%)	0 (0%)
	Total	19	17 ((20%))	66 ((80%))	0 ((0%))
100-225	-/-	30 [23%]	25 (88%)	5 (12%)	0 (0%)
	+/-	57 [44%]	0 (0%)	31 (54%)	26 (46%)
	+/+	42 [33%]	0 (0%)	7 (17%)	35 (83%)
	Total	129	25 (19%)	43 (33%)	61 (47%)

* Only a subset of control embryos were genotyped (to ensure reproducibility).

§ Percentages in curved brackets represent fraction of embryos of indicated genotype showing listed *myod* expression pattern.

¶ Percentages in square brackets represent fraction of embryos in sample with each genotype.

∞ Percentages in double brackets represent fraction of embryos in sample showing listed *myod* expression pattern.

bioRxiv preprint doi: https://doi.org/10.1101/766501; this version posted September 12, 2019. The copyright holder for this preprint (which was not certified by peer review) is the author/funder, who has granted bioRxiv a license to display the preprint in perpetuity. It is made available under aCC-BY-NC-ND 4.0 International license.

Fig. S1. Expression of *aplnrb* mRNA during zebrafish axis formation.

Wholemount in situ mRNA hybridization of apelin receptor b *(aplnrb)* mRNA in zebrafish embryos at the indicated stages, shown in animal (An), lateral (La), dorsal (Do, animal to top), ventral (Ve, animal to top) and posterior (Po, dorsal to top) views. Ant = anterior. Note significant expression in early germ ring (arrows), future cranial mesoderm (large and small brackets highlight comparable regions of expression) and adaxial cells (arrowheads). Expression is lacking in paraxial mesoderm (white dashes) that expresses *myf5* and later *myod* mRNAs (see Fig. 1C).

Fig. S2. MRF over-expression rescues trunk slow myogenesis.

Confocal stacks showing immunodetection of slow fibres with Slow MyHC in *smo* mutant (identified by lack of tail circulation), *smo* sibling, un-injected control or cyA-treated embryos injected with *myod* or *myog* RNA. All embryos orientated anterior to left dorsal up showing 2-3 trunk somites (A-H) or entire trunk and tail (I,J). **A,B.** *Myod* RNA-injected *smo* siblings have slow muscle with disrupted somite morphology**. C,D.** Rare slow fibres present in the trunk region of *smo* mutants (arrow) are more common after *myod* RNA injection. **E,F.** CyA-treatment prevents slow fibre formation. Presence of maternal Smo protein may account for the greater number of residual slow fibres in *smo* mutant compared to cyA-treated embryos. **G,H.** *Myod* or *myog* RNA injection rescues slow fibre formation in cyA-treated embryos. Inset in H shows co-expression of slow MyHC, Prox1 and GFP in a cyA-treated embryo after injection of *myog-IRES-GFP* RNA. **I,J.** *Myog* RNA rescues slow fibres in trunk but not tail. Insets show co-expression of Prox1 and slow MyHC in short confocal stacks. **K.** Slow fibres were counted at 24 hpf in each somite of seven control *smo* mutants and seven *smo* mutants injected at 1 cell stage with *myod* RNA. **L.** Slow fibres were counted at 24 hpf in each somite of ten control uninjected and ten embryos injected at 1 cell stage with *myog* RNA that were each subsequently treated with cyA from 30% epiboly. Bars: 50 μm.

bioRxiv preprint doi: https://doi.org/10.1101/766501; this version posted September 12, 2019. The copyright holder for this preprint (which was not certified by peer review) is the author/funder, who has granted bioRxiv a license to display the preprint in perpetuity. It is made available under aCC-BY-NC-ND 4.0 International license.

Fig. S3. *Dorsal fgf expression and requirement for adaxial myogenesis.*

In situ mRNA hybridization for fgfs in wild type embryos at 80% epiboly, tailbud (tb) and 6ss (A), for *myod* and *myf5* in control and fgf MO-injected and *fgf8a*$^{-/-}$ embryos at 80% (B,C) and for *tbxta* (red) and *myod* (blue/brown) (D). **A.** *fgf8a, fgf4*, *fgf6a* and *fgf3* transcripts appear successively in wild type embryos in the dorsal midline (arrows) and CNH (arrowheads). **B.** *Myod* and *myf5* mRNAs in *fgf3* MO, *fgf4* MO and *fgf6a* MO wild type embryos and in sequence-genotyped *fgf8a*$^{-/-}$ embryos at 80% epiboly (upper rows, con and single MOs from a representative experiment). Note that siblings of the *fgf8a* mutants had similar MRF expression. Arrowheads indicate nascent adaxial cells. **C.** *Myf5* mRNA in sibling embryos from an incross of heterozygous *fgf8a*$^{+/-}$ fish injected with 6 ng control MO or 2 ng each of *fgf3*, *fgf4* and *fgf6a* MO. Note the successively stronger reduction in signal as more fgf function is removed. **D.** Rows showing replicate fgf MO-injected embryos had reduced accumulation of *myod* mRNA in pre-adaxial cells of compared to control (con) (arrowheads). Note widening of notochord in *fgf6a* morphants. Bars: 100 μm.

Fig. S4. *Aplnrb* mRNA changes in Tbx mutants.

In situ mRNA hybridization for *aplnrb* in wild type sibling and *tbx16* mutant and *tbxta* mutant embryos at 80% epiboly. Single embryos are shown from dorsal, left lateral and ventral views. Labelling (brackets) is in a band of anterior mesoderm. Note the unlabelled region in wild type and *tbxta* mutant that is missing in *tbx16* mutant (white dashes). Adaxial *aplnrb* mRNA up-regulation (arrowheads) is lacking in mutants.

Fig. S5. ChIP-seq analysis of *myod* locus.

ChIP-seq on wt embryos at 75-85% epiboly indicates endogenous Tbx16 and Tbxta binding events within 75 kb flanking *myod* TSS. H3K4me3 marks TSSs; H3K4me1 marks enhancers; H3K27ac indicates active enhancers; RPM – ChIP-seq peaks height in reads per million reads. Multiz Alignments & Conservation from UCSC Genome Browser (Haeussler et al., 2019) are shown beneath. Purple boxes indicate significant Tbx binding for Tbx16 and Tbxta (DDE1) and Tbxta alone (DDE3). Cyan boxes indicate of Tbx sites mentioned in text. Significant H3K4me1 marks are present at both DDE1 and DDE3, while only DDE3 has a significant H3K27ac mark.

Fig. S1

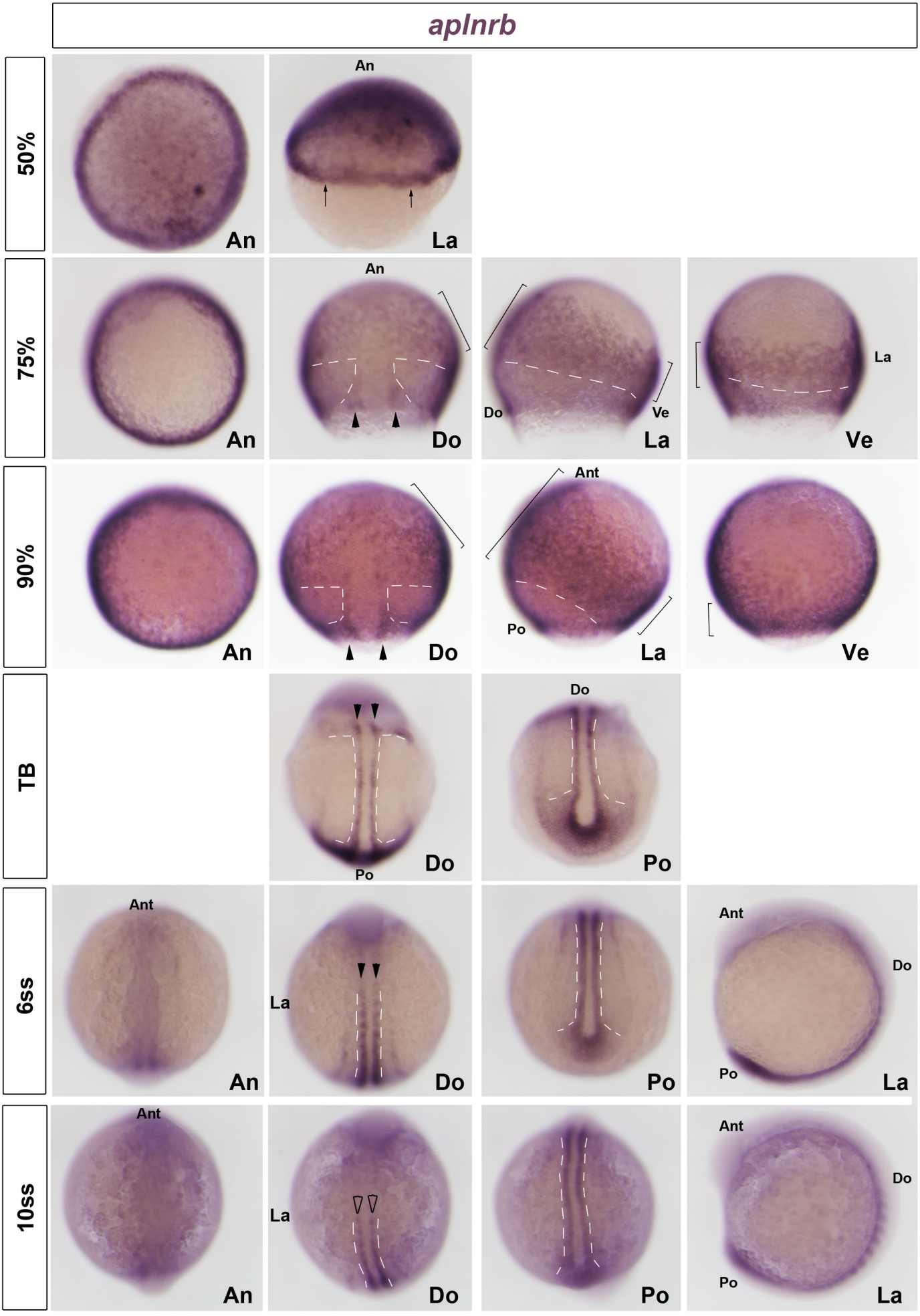
aplnrb
50%
An
La
75%
An
Do
La
Ve
90%
An
Do
Ant
Po
La
Ve
TB
Do
Po
6ss
Ant
An
La
Do
Po
Ant
Do
Po
La
10ss
Ant
An
La
Do
Po
Ant
Do
Po
La

Fig. S2

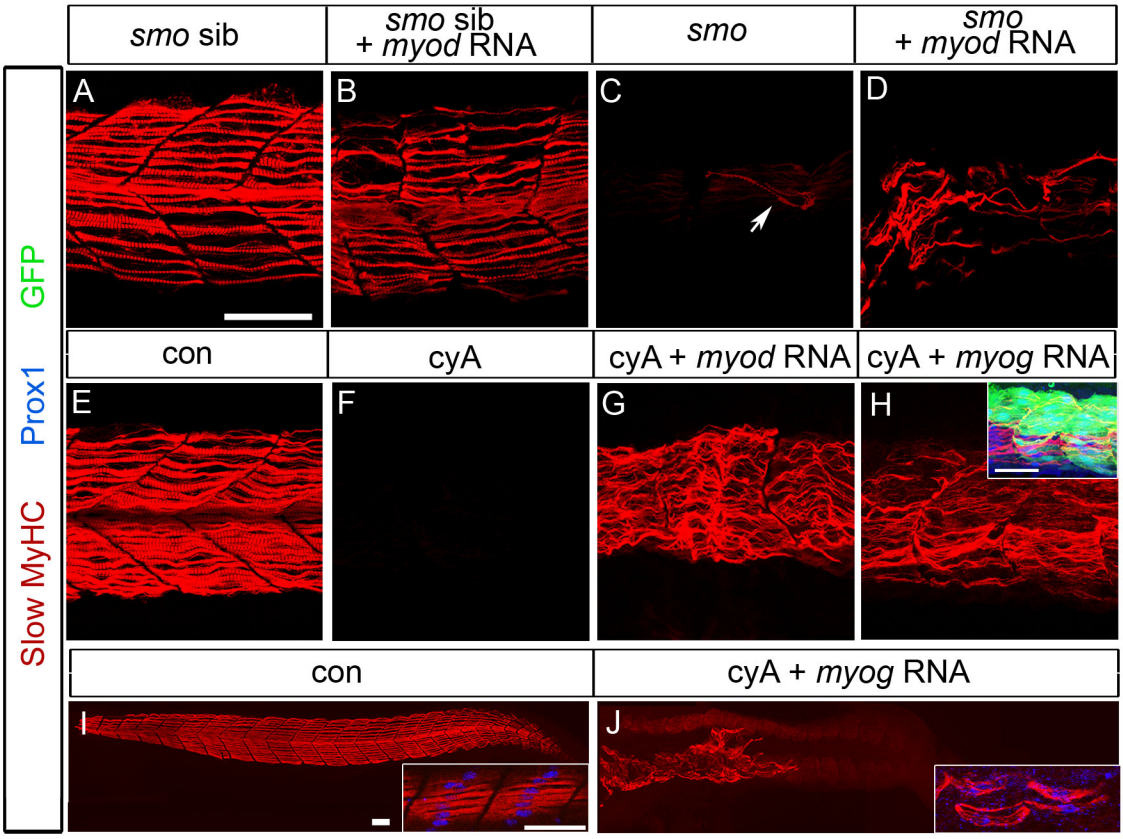
smo sib
smo sib + myod RNA
smo
smo + myod RNA
A
B
C
D
GFP
Prox1
Slow MyHC
con
cyA
cyA + myod RNA
cyA + myog RNA
E
F
G
H
con
cyA + myog RNA
I
J

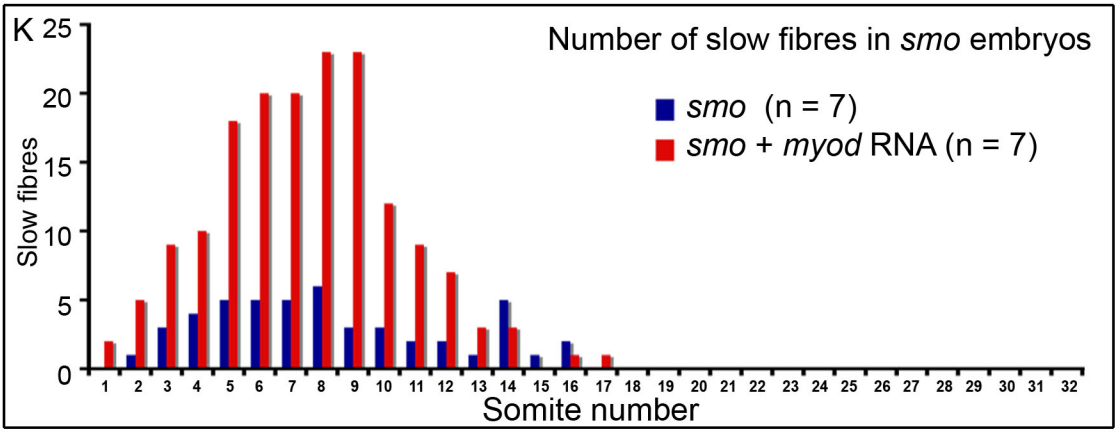
K
Number of slow fibres in smo embryos
smo (n = 7)
smo + myod RNA (n = 7)
Slow fibres
Somite number

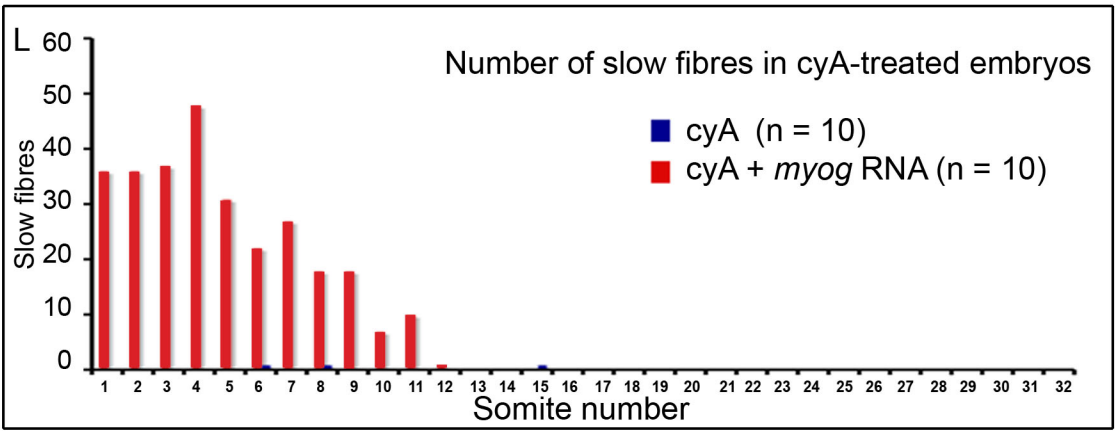
L
Number of slow fibres in cyA-treated embryos
cyA (n = 10)
cyA + myog RNA (n = 10)
Slow fibres
Somite number

Fig. S3

bioRxiv preprint doi: https://doi.org/10.1101/766501; this version posted September 12, 2019. The copyrig
was not certified by peer review) is the author/funder, who has granted bioRxiv a license to display the p
available under aCC-BY-NC-ND 4.0 International license.

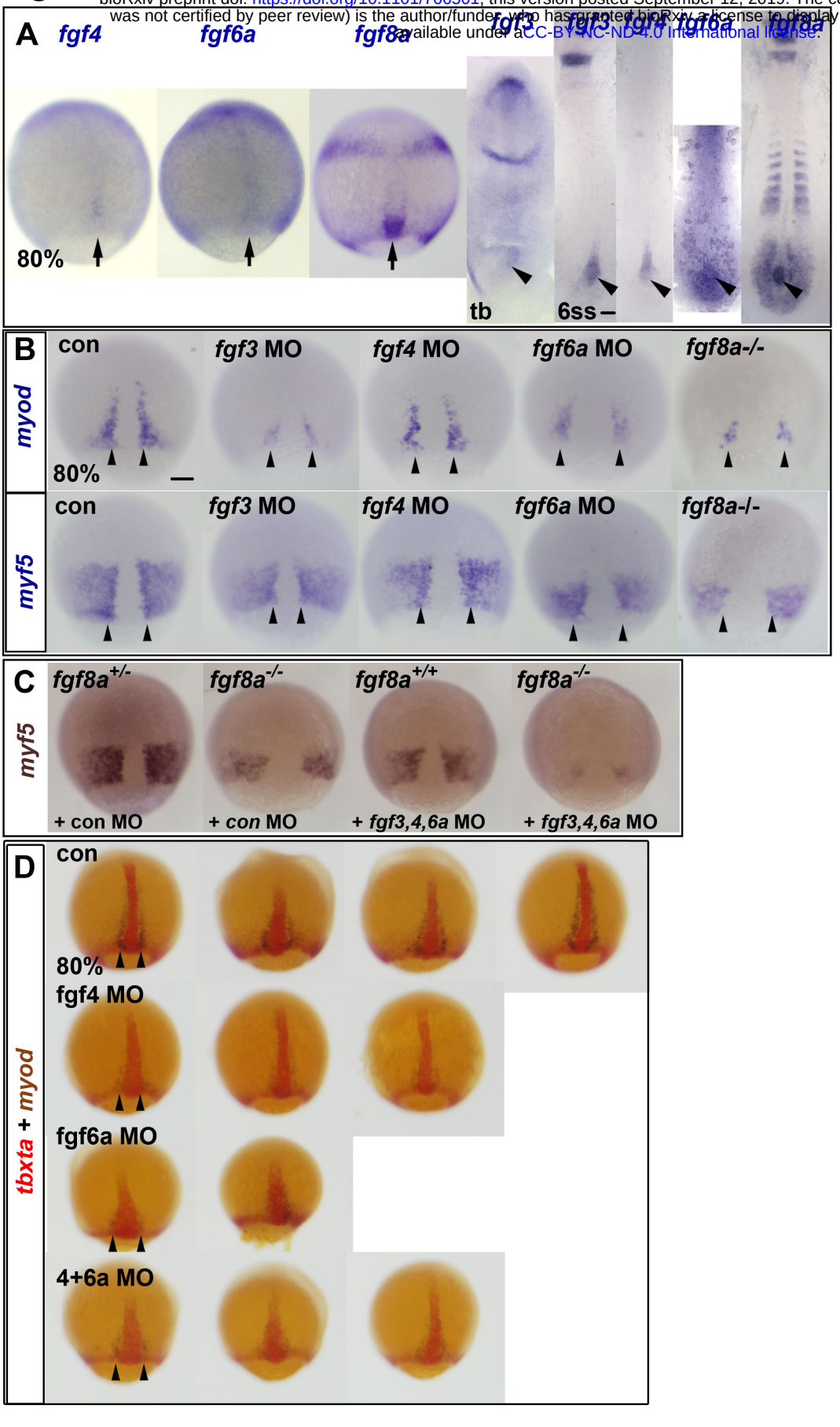

bioRxiv preprint doi: https://doi.org/10.1101/766501; this version posted September 12, 2019. The copyright holder for this preprint (which was not certified by peer review) is the author/funder, who has granted bioRxiv a license to display the preprint in perpetuity. It is made available under aCC-BY-NC-ND 4.0 International license.

Fig. S4

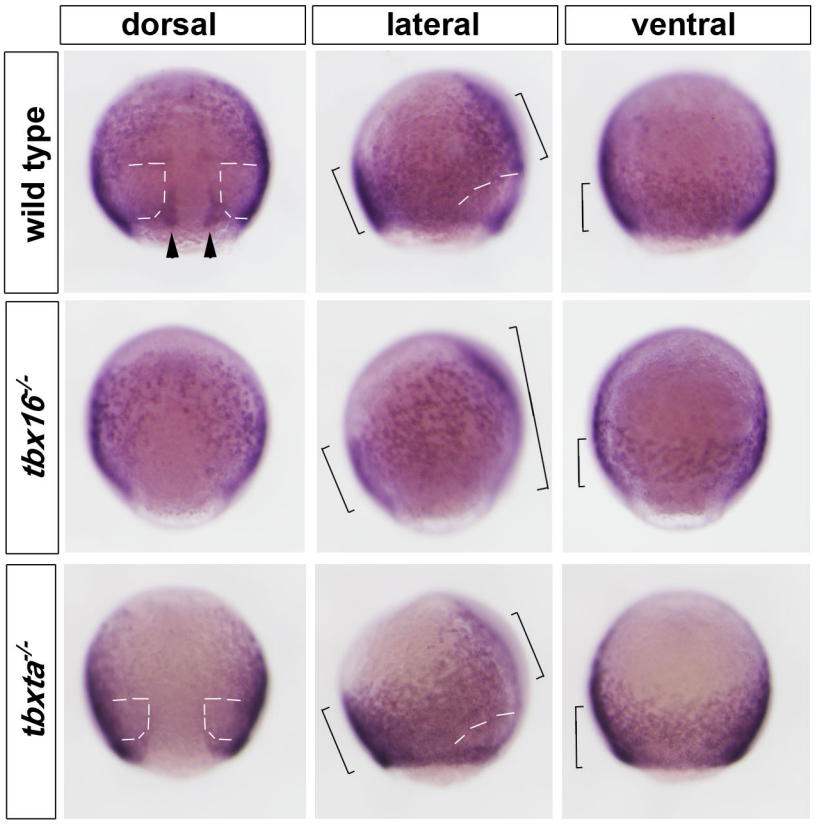

Fig. S5

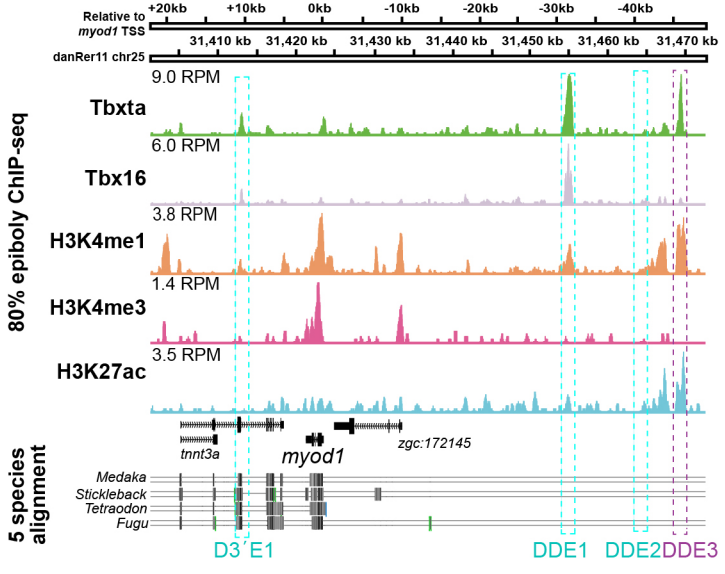
Relative to myod1 TSS
+20kb
+10kb
0kb
-10kb
-20kb
-30kb
-40kb
danRer11 chr25
31,410 kb
31,420 kb
31,430 kb
31,440 kb
31,450 kb
31,460 kb
31,470 kb
80% epiboly ChIP-seq
9.0 RPM
Tbxta
6.0 RPM
Tbx16
3.8 RPM
H3K4me1
1.4 RPM
H3K4me3
3.5 RPM
H3K27ac
tnnt3a
myod1
zgc:172145
5 species alignment
Medaka
Stickleback
Tetraodon
Fugu
D3
E1
DDE1
DDE2
DDE3